Alterations in ecosystem water cycle associated with land-use changes under different precipitation regimes

M.Sc. Thesis

Submitted to the Robert H. Smith Faculty of Agriculture, Food and Environment

The Hebrew University of Jerusalem

For the Degree
'Master of Agricultural Science'

By
Shani Rohatyn

Rehovot January, 2017

This work was done under the supervision of

Dr. Eran Tas
The Robert H. Smith Faculty of Agriculture, Food and Environment,
The Hebrew University of Jerusalem, Rehovot, Israel

and

Prof. Dan Yakir
Weizmann Institute of Science, Rehovot, Israel

Acknowledgment

I would first like to thank my advisors, Prof. Dan Yakir and Dr. Eran Tas, for all the support during the past three years. You were always there when I needed the help, first to develop my own research questions and working plan, later with guidance in challenging periods throughout the fieldwork and data processing and finally with the help of collecting it all to one interesting scientific story presented in this thesis. Dan and Eran, I thank you for giving me this unique opportunity to study topics I love and interested in, and to have an ideal combination of intensive fieldwork next to complex data processing and science studies.

I would also like to thank Dr. Eyal Rotenberg, who was there for me through all my studies years, supporting me in both scientific and emotional levels. Thanks a lot for never giving up on me and for always believing I have the ability to be a good scientist. Eyal, you were a very important part of this research and I appreciate much the opportunity to work with you.

Thanks to Efrat Ramati, for working with me on the mobile lab system and data processing, with a lot of passion and enthusiastic, for many long filed days together, for good food and always high spirit. Thanks to Yoav Rubin, for working with me on the intensive field days, from sunrise until sunset, and helping with the mobile systems and data processing. Thanks to Fyodor Tatarinov for working with me on the data processing, always answering to my request, even when they are challenging and time consuming, and never complaining. Fyodor, I would definitely could not done this without you.

Thank for all the group members from both the Faculty of Agriculture and the Weizmann Institute of Science along the years- Yakir, Efi, Efrat, Fyodor, Gil, Fulin, Rafat, Rafael, Jonathan, Yoav, Maor and Moshe, for making the office and filed feel like home, with good food and supportive environment. Thanks to all the research assistant students- Tamar, Shaked, Leyla, Madi, and Omri.

I would like to thank to my family, parents and sisters, for never-ending emotional support, and a last big thank to my partner for life, Nir, who is always there for me, when I straggle, when I question myself, for believing in me like no one else does.

List of symbols and abbreviations

ICG	Israeli Climatic Gradient
HM	Humid-Mediterranean study sites
M	Mediterranean study sites
SA	Semi-Arid study sites
F	Forest ecosystem
NF	Non-forest ecosystem
IMS	Israeli Meteorological Data
FMA	Flux Meteorological Algorithm
Ta	air temperature (ºC)
RH	relative humidity (%)
Rg	global incoming shortwave radiation (W m^{-2})
VPD	atmospheric vapor pressure deficit (Pa)
VPDL	leaf level vapor pressure deficit (Pa)
P	precipitation (mm)
ET	evapotranspiration (mm)
WY	water yield (mm)
WYe	ecosystem water yield (mm)
R	overland flow- runoff (mm)
GR	groundwater Recharge (mm)
ΔS	changes in soil water content (mm)
E_s	soil evaporation (mm)
T	transpiration (mm)
SF	sap flow rate (l hr^{-1})
SFD	sap flux density (cm^3 cm^{-2})
g_s	leaf scale stomatal conductance to water (mol m^{-2})
g_w	canopy scale stomatal conductance to water (mol m^{-2})
LE	latent heat flux (W m^{-2})
H	sensible heat flux (W m^{-2})
G	soil heat flux (W m^{-2})

GPP	gross primary production (gC m^{-2})
PET	potential evapotranspiration (mm)
D	seasonality index- 'transpiration deficit' (mm)
R_a	air resistance within the inertial sublayer (m s^{-1})
R_b	roughness sublayer resistance (m s^{-1})
R_s	surface resistance including stomatal and non-stomatal resistances (m s^{-1})
G_s	surface conductance, $1/R_s$ (s m^{-1})
ρ	air density (kg m^{-3})
C_p	heat capacity (J K^{-1} kg^{-1})
λ	latent heat of vaporization (J kg^{-1})
γ	psychometry constant (Pa K^{-1})
F_{O3tot}	total ozone flux (µmol m^{-2})
F_{O3sto}	stomatal ozone flux (µmol m^{-2})
F_{O3ns}	non-stomatal ozone flux (µmol m^{-2})
T_{gw}	transpiration derived by stomatal conductance to water (mm)
T_{SF}	transpiration derived from up scaled sap flow measurements (mm)

Abstract

Vegetation and soil can emit in water vapor by evapotranspiration (ET) in quantities equivalent to the entire annual local precipitation (P). This can greatly impact the local hydrology, leaving a small residual [P-ET], termed ecosystem water yield (WYe) in the fresh water that is available for human consumption. The general objective of this study is to examine the interactions between land-use change (from sparse shrub land to pine forest) and precipitation regime (from humid Mediterranean to semi-arid conditions) on WYe, and to identify the mechanisms underlying these interactions. We hypothesized that forestation increases ET and therefore reduces WYe by increasing the transpiring leaf area and root depth, but this effect diminishes with decreasing precipitation.

We used a new custom-built mobile laboratory that was deployed on a campaign basis (about two weeks per site, repeated along the seasonal cycle), which allowed us to measure ecosystem-scale ET together with carbon, energy and ozone fluxes, as well as meteorological parameters. Measurements were carried out from 2012-2015 in three paired sites of *Pinus halepensis* forests and adjacent non-forest ecosystems along the rainfall gradient in Israel, ranging from 755 to 285 mm of annual precipitation. The extension of the campaign results to annual ET is based on multiple-regression analyses with continuous meteorological records from local meteorological stations, using the Flux-Meteorological-Algorithm. The physiological parameters, such as transpiration (T) and stomatal conductance (g_s) were estimated using sap flow (SF) sensors and gas-exchange leaf chamber respectively.

In dry conditions, WYe was small and the forest impact was limited, reducing WYe from 70 mm in the non-forest ecosystem to 12 mm in the forest ecosystem (-58 mm). Under wetter conditions, the forestation effect was greater, reducing WYe from 344 to 144 mm (-200 mm). This was mostly due to the greater increase in ET from the dry to the wetter forest (from 267 to 583 mm or x2.2), compared to the non-forest areas (from 216 to 383 mm, or x1.8). The phenology of ET also changed, with the forest peak ET shifting from early March in the dry site to late May in the humid sites and with the non-forest peak ET shifting from late February in the dry site to late March in the humid site. The seasonal campaigns show changes in the diurnal pattern of measured water fluxes at all scales (ET, T and g_s) in response to changes in climatic conditions, thereby indicating differential environmental effects (e.g., global radiation and water-vapor pressure deficit) and physiological control (e.g., g_s and SF).

We concluded that afforestation is always associated with a loss in Wye, due to increased ET, but that the afforestation impact on WYe is non-linear, with diminishing effects in water-limited environments and approaching a higher and constant effect (with ET reaching a maximum) in wet environments. In this work, we 1) demonstrated a new measurements approach based on the mobile lab; 2) developed and validated the Flux-Meteorological-Algorithm; 3) based on 1 & 2, provided the first quantitative results of the effects of land-use changes on the local hydrology under increasingly drying conditions, as predicted for our region. This study indicates that, while the hydrological impact of forestation in humid Mediterranean conditions is important to consider, the benefits of forestation in increasingly drying conditions (soil protection, surface cooling, wood production and so forth) may outweigh the diminishing hydrological impact.

Table of Contents

1 Introduction

1.1 Forests under climate change, globally and locally

It is generally expected that the increase in greenhouse gases (GHG) due to anthropogenic activities will result in global environmental changes and alterations in climate systems. In the past 200 years since the industrial revolution, changes in the atmosphere's composition already increased the Earth's surface temperature by over 1˚C and will likely exceed 1.5°C by 2100 (IPCC, Pachauri *et al.*, 2014).

In attempting to predict the future climate on Earth, it is essential to understand the complex interactions between ecosystems and climate change. Through physical, chemical and biological processes, forest ecosystems (which comprise ~30% of the land cover) can enhance or diminish climate change (Bonan, 2008). For growth and survival, vegetation consumes carbon from the atmosphere a process leading to water transpiration, using water originating from the soil layer. When combined, this essential gas-exchange process, which is carried out continuously by each individual plant, has a major effect on the global biogeochemical cycles (e.g., carbon and water). For example, forests sustain the hydrologic cycle through evapotranspiration, which cools the surface and transfers moisture and energy (latent heat) to the upper troposphere, thereby enhancing cloud formation and precipitation, which are associated with energy release during vapor condensation.

Climate change affects vegetation function and productivity significantly and in many ways, including changes in water supply, air temperature and the increase in atmospheric CO_2 concentration, all of which have the potential to affect plant transpiration: one of the largest components of the hydrological cycle (McVicar *et al.*, 2010). The increase in drought intensity can lead to lower growth rates and eventually to higher tree mortality, which is associated with physiological failure (McDowell *et al.*, 2008), or fire and other disturbances (Dale *et al.*, 2001). Forests' survival requires adaption, not only to changes in mean climate variables, but also to increased variability with greater risk of extreme weather events (Lindner *et al.*, 2010). Dry regions, such as the Mediterranean region, are expected to be under limited water conditions (Giorgi and Lionello, 2008) and increased fire risks (Moriondo *et al.*, 2006), which may result in plant adaptations and physiological responses.

The *Pinus halepensis* (Aleppo pine) is a common species in the Mediterranean region and is considered to be a drought-resistant species (Ne'eman and Trabaud, 2000). Over the past decades, population growth has changed the nature of Israel's land cover. One of these changes is the afforestation of shrub lands and grasslands, mainly by the Jewish National Fund of 'Keren Kayemeth LeIsrael' (JNF-KKL), which increased Israel's forest area more than fivefold, from 30,000 to 160,000 hectares between 1960 and 2011 (Israel CBS, 2014). Despite forests' strong impact on water balance and although Israel's water resources are of high importance, there is still a lack of research regarding the impact of afforestation on the water that is available for human needs.

1.2 The hydrological cycle and its components

The annual hydrological cycle can be described as the water balance between Earth's surface and the atmosphere. In more detail, water that is supplied to the land through rainfall is either transported back to the atmosphere by the processes of evaporation from soil (E_s) and plants (T), or continue as overland flow (runoff, R) or infiltration, into the ground-water reservoir (G, which, in turn, indicates runoff or evaporation fluxes on a longer time scale).

The hydrological cycle is aptly simplified in the following equation (e.g., Zhang *et al.*, 2001):

$$P = ET + R + GR + \Delta S \quad \text{(mm)} \qquad (1)$$

where P is balanced by the sum of ET, runoff (R), recharge to ground water (GR) and changes in soil-water content (ΔS).

The precipitation input is largely stochastic in duration and amount at a local scale (e.g., Trenberth *et al.*, 2003). The spatial variability increases as the climate becomes drier and more controlled by convective rain cells that lie far from the center of the storm (Noy-Meir, 1973). Rainfall can either reach the ground by through-fall or evaporate from plants by interception. The extent of the interception component depends on the vegetation type and density, rain intensity and meteorological parameters (Gash, 1979).

Evapotranspiration is the transportation of water from soil (E_s), plant surface (Interception, I,) and through the plants and their leaves (T), which in the gaseous phase is described as follows:

$$ET = E_s + T + I \ (mm) \qquad (2)$$

The required energy for evaporation, the latent heat (LE), originates directly or indirectly from global solar radiation (Rg). Daytime atmospheric turbulence is important in transporting moisture from the surface, thereby influencing the overall evaporation flux. The driving force for ET is the difference between the amount of moisture in the air (e_a) and how much moisture the air can hold when it is saturated (e_s), and is a measured parameter that is known as vapor pressure deficit (VPD). The soil's properties, the plant hydraulic conductance and the water content define the availability of water for ET. Plant physiology is also important in controlling transpiration through stomatal conductance (g_s) to water-vapor flux, thereby controlling the amount of water that the plant will lose. When VPD is high and soil-water availability is low, plants can minimize their water loss by closing stomata and reducing stomatal conductance. This regulation process is expressed in the observed changes in the diurnal cycle of plant activity and can adapt to harsh conditions, for instance by shifting peak activity periods to early morning or late afternoon, thereby reducing loss of water (Collatz *et al.*, 1991; Dzikiti *et* al., 2007; Klein *et al.*, 2015).

Water that is not lost in evaporation but returns to the atmosphere can flow under and above the soil surface. Infiltration to depth can occur when soil is saturated and when soil resistance to water transport is low. Water flow that cannot infiltrate into soil and is not evaporated, creates overland flow, termed runoff (R).

1.3 The importance of water resources under global warming, population growth and land-use change

Global warming has already resulted in changes in the water cycle and these effects will likely intensify due to higher evaporation rates, and larger atmosphere vapor-holding capacity (Ohmura & Wild, 2002). Although the above assumption is generally accepted, terrestrial observations over a period of 50 years show the reverse response of decreasing evaporation rates, as expected from large and widespread decreases in sunlight that result from increasing cloud coverage and aerosol concentration (Roderick & Farquhar, 2002). These two controversial responses demonstrate the importance of better understanding the changes in evaporation rates due to climatic change. Moreover, changes in the water cycle also include changes on a global scale in precipitation patterns over land (with the general trend of wet regions becoming wetter and dry regions becoming drier) and the intensification of heavy precipitation events in

some regions (Huntington, 2006). The predictions of future global warming and changes in precipitation will not be uniform around the globe. While in the high latitudes, precipitation is expected to increase, the mean precipitation in mid-latitude dry regions is more likely to decrease (IPCC, 2014). Specifically, according to Giorgi and Lionello's (2008) review of future climate changes in the Mediterranean region, it expected that this region will experience a decrease in precipitation in the dry season, an increase in inter-annual variability and a pronounced warming, leading to its recognition as a climate change "hot spot" (Giorgi, 2006; IPCC, 2007; Lelieveld *et al.*, 2012). Moreover, climate models for the region of Israel predict an increase in winter temperature combined with changes in rainfall amount and distribution (Ben-Gai *et al.*, 1998).

Global climate change predictions indicate that freshwater resources are vulnerable and have the potential to be strongly impacted by the future climate, with wide-ranging consequences for human societies and ecosystems. Changes in extreme events, such as floods and droughts, are not only expected to have an impact on the quantity of available freshwater, but also on its quality, with a possible negative impact on ecosystems and human health (IPCC, 2008). In addition, the salinization of groundwater in the coastal area is expected to expand due to the increase of sea levels. Globally, by the 2050s, 75% of the river-basin areas are expected to be under increased water stress and to decrease in freshwater availability. The increase of R and the availability of freshwater in some areas will probably be overcome by the negative effects of an increased precipitation variability and seasonal R shifts in water supply, water quality and flood risks (IPCC, 2008).

In considering future changes in water availability, it is important to also include future increases in water demand due to population growth and economic development. Previous global water-cycle research shows that changes in water demand will have a far greater effect on water availability than global climate change and demonstrate the need to understand the interactions between the two (e.g., Vörösmarty *et al.* 2000; Alcamo *et al.,* 2007). Among several changes, population growth has and will continue to have a strong impact on land-use changes, including the expansion and intensification of agriculture, the growth of urban areas, and changes in vegetation cover (DeFries & Eshleman, 2004).

The water that is available for human use is related to the hydrological cycle through the 'water yield' (WY), defined as the total outflow from a drainage basin, either through surface channels or to subsurface aquifers within a given time (e.g., annually; Farley *et al.*, 2005; Ellison *et al.*, 2013 and references therein). In practice, WY is equated with measured R and ground-water recharge (WY=R+G; eq. 1) in a system, on annual or longer time scales in which soil water changes can be assumed to be negligible (i.e., ΔS lies near zero). Its estimate is often simplified (e.g., Bren *et al.*, 2006; Oki & Kanae, 2006) with the following equation:

$$WY = P - ET \quad (2)$$

While hydrological balance is often considered on the basis of a drainage basin or watershed, it can also be considered on the basis of an ecosystem, if it can be hydrologically distinct, in which case it could be indicated as WYe. Dryland ecosystems, which are the focus of this study, often depend solely on current-year rainfall (e.g., Huxman *et al.*, 2005; Raz-Yaseef *et al.*, 2010) and can be characterized as a 'closed system', with ET accounting for nearly the entire annual precipitation and with minimal water storage between years.

Through the process of ET, forests, among other vegetation types, affect the water balance and WYe. Yet, the direction of this effect is not well quantified (Ellison *et al.*, 2012) and depends on climatic conditions (Creed *et al.,*2014). By means of their developed root system, forests also change soil properties, such as their conductivity to water, and further partition the remaining WYe between infiltration into the soil and flow above the ground. Ultimately, however, both components can be used by humans, if treated properly (e.g., Bronstert *et al.*, 2002; Cerdà, 1998). Therefore, estimating the dominant flux in equation 1, ET, and better understanding the impact that factors such as climate and land-use change have on it, can help in predicting future changes in local and global water balance and WYe.

Previous research shows that afforestation increases soil-hydraulic conductivity, as well as increased infiltration rates and decreased surface R, thereby decreasing the WY while, but also avoiding damages from extreme flood events (Farley *et al.*, 2005; Kundzewicz, 1999). Farley *et al.* (2005) reported that the afforestation of grassland and shrub land reduced R by 44% and 31% respectively, with significant effects depending on the tree species (Eucalyptus trees reduced R by 75%, while pine trees reduced R only by 40%). Moreover, by increasing the transpiring leaf area and with the greater access of the trees' roots to deeper soil layers,

afforestation could lead to greater loss of water into the atmosphere by ET, and therefore lower levels of WY. The issue regarding the impact of changes to vegetation cover on water yield was well demonstrated at the Hubbard Brook experimental forest, in New Hampshire. The results of this research indicate an initial increase in water yield after forest cutting, followed by a decrease due to forest regeneration (Campbell *et al.,* 2007). Shachori and Michaeli (1965) assessed the potential annual water availability based on a simple model of linear regression in the Western United States, which has vegetation and climate conditions that are similar to those in Israel (200 - 1400 mm). The study shows statistically significant differences between areas with or without vegetation cover. The WY in areas with non-woody plant covers was higher due to the fewer roots and lower transpiration rates (Shachori *et al.*, 1965). Based on this work, Stanhill (1993) shows that tree covers in our region decrease the amount of available water by up to 10%, compared to that obtained from herbaceous covers under the same climatic conditions. On the other hand, basin-level measurements in the Northern desert of Israel show that the mean annual R from bare-soil basins were only a few percent higher than those from forest-covered areas (Alexandrov *et al.*, 2008).

1.4 Partitioning the Evapotranspiration flux

Understanding the mechanism underlying forest-water use can improve local and global predictions for the availability of water under changing land use and climatic conditions. ET is usually treated as a single entity. However, it is critical to partition the ET flux (eq. 2) into its components, in order to better understand the interactions between each component and the vegetation types, as well as the environmental and climatic parameters. The partitioning of ET is commonly done by estimating the total ET flux and, independently, one of its dominant components, T or E_s. The capability to carry out ET-flux partitioning has wide-ranging implications for local water availability, plant growth, carbon assimilation and soil respiration, for instance (Raz Yaseef *et al.*, 2010). Such information is important in predicting the consequences of ecosystems' response to future climate change, the effects of deforestation, management and decision-making.

The partitioning of ET into its two main components begins with its original driving force, VPD, which is the atmospheric demand for vapor relative to the water content of the soil, i.e. the driving force for ET and hydraulic conductivity. The latter is intrinsic to the soil in referring to E_S

and to the soil-root-leaf continuum in referring to T. The relation between the evaporative fluxes and VPD can be demonstrated by the evaporation equation (e.g., Jones 1998):

$$E = g_w * (e_s - e_a) * \left(\frac{0.622\rho_a}{P_a}\right) \quad (3)$$

where E is the desired evaporation flux T (in the current case in kg m^{-2} s^{-1}), g_w is the stomatal conductance to water at the canopy scale in m s^{-1}, e_s is the saturated vapor pressure for the atmospheric temperature (Pa) and e_a is the actual vapor pressure (Pa). The difference between the previous two is equal to atmospheric vapor-pressure deficit (VPDA) and the final term is unit conversion, which includes air density, ρa in kg m^{-3} and air pressure in Pa.

Notably, while E_s is a physically controlled system, T is biologically controlled and can be affected by factors such as plant disease, atmospheric CO_2 concentration and soil fertilization. Semi-arid landscapes represent a transition zone between humid environments, in which water availability is high and woody plants can be expected to have a large effect on the water budget, and arid ones, in which water resources are limited, and vegetation cover is very low and has a minimal effect on R (Huxman *et al.*, 2005). The relationship between vegetation cover and the water budget in these transition zones is complex and poorly understood.

2 Objectives

The main objective of this study is to quantify the change in the differences in the water balance between forested and non-forested ecosystems along the Israeli Climatic Gradient (ICG).

2.1 The specific objectives:

a. To develop the means for using campaign-based data (1-2 weeks of continuous data for each season) as the basis for evaluating continuous annual ET flux in different sites, based on the relationships between meteorological and ecosystem-flux data.

b. Using the methodology in 'a' and a newly developed mobile laboratory, to examine the seasonal and annual-scale interactions between the effects of land use (sparse shrub land and pine forest) on ecosystem water yield and the changes in the precipitation regime (from humid Mediterranean to semi-arid conditions).

c. To identify the driving mechanisms underlying the changes in the water cycle occurring along the climatic gradient and between different land covers.

2.2 The main working hypotheses:

a. By increasing the transpiring leaf area and root depth, forestation increases ET and therefore reduces ecosystem WY, but this effect diminishes with decreasing precipitation.

b. Using high resolution flux-data sets obtained from short-term measurement campaigns in different seasons and under different meteorological conditions is an efficient research tool by which to estimate and evaluate continuous fluxes, and annual-scale fluxes.

c. When water is a limited factor, the increase in precipitation results in an increased canopy conductance to water (g_w) and transpiration (T), thereby leading to higher T/ET ratio.

3 Materials and Methods

3.1 Study sites description

The study was carried out in Israel at the edge of the arid region, along the steep Israeli climatic gradient (ICG; Fig. 2.1). Field campaigns of 2-3 weeks each were carried out during 2012-2015 in three planted mature Aleppo pine forests (*Pinus halepensis*), and their adjacent non-afforested ecosystems, and in one oak forest site. The selected sites (see Fig. 2.1 and table 2.1) included a dry semi-arid (SA) site, in the Yatir forest (mean annual precipitation of 280 mm), which is a permanent flux-tower site with continuous long-term flux measurements and part of the global flux network (http://fluxnet.ornl.gov). An intermediate dry Mediterranean (M) site, was in the Eshtaol forest (mean annual precipitation of 520 mm), a humid Mediterranean (HM) site was in northern Israel at the Birya forest (mean annual precipitation of 710 mm). An oak stand site was located in the Ha'solelim forest in the western Galilee (Mediterranean, M, climate with mean annual precipitation of 580 mm), with mixed oak forest dominated by *Quercus calliprinos* (evegreen) and *Q. ithaburensis* (deciduose) accompanied by small proportion of other Mediterranean broadleaved tree and shrub species. Non-forested sites were selected adjacent to the forest sites and were all exposed to continuous livestock grazing with the vegetation structures reflecting both the local climate and grazing regime (see Table 2.1 for more study site information).

3.2 Mobile laboratory

To extend measurements beyond the permanent Yatir flux tower site, a newly designed mobile flux measurement system was used on campaign basis in all other sites. The mobile lab was based on adjustable 4-28m pneumatic mast on a 12-ton 4x4 truck and a complete eddy flux system and enclosed laboratory space (Fig. 2.2). The laboratory provided an air-conditioned instrument, power and communication facility. Non radiative fluxes measurements rely on the eddy-covariance (EC) system used to quantify CO_2, sensible (H) and latent heat (LE) fluxes using a three-dimensional sonic anemometer (R3, Gill Instruments) and an enclosed-path CO_2/H_2O infrared gas analyzer (IRGA; LI-7200, LI-COR Inc., Lincoln, NE, USA) with 60 cm long tubing fitted with 2 μm filter at the inlet (F series, Swagelok, US). Deployment and data analysis was based on CarboEuroflux methodology (Aubinet *et al.*, 1999). Air temperature and relative humidity (HMP45C probes, Campbell Scientific Inc. Utah) and air pressure (Campbell Scientific sensors Inc. Utah) were measured 3-5m above the canopy. Radiative fluxes were measurements included solar radiation (0.285-2.80 μm; CMP21, Kipp and Zonen, The Netherland), long-wave radiation (4.5-42 μm; CGR4, Kipp and Zonen, The Netherland) and photosynthetic radiation (PAR, 0.4-0.7 μm; PAR-LITE2) sensors. All sensors were installed in pairs facing both up and down, and were connected using differential mode through a multiplexer to a data logger (CR3000, Campbell Scientific Inc. Utah). Meteorological variables (Temperature, T, and relative humidity, RH) and the radiation components (solar radiation, long-wave radiation, and PAR) were sampled at 1Hz, and processed, with averages stored every 30 minutes on the CR3000 data logger. Mean 30-min non-radiative (CO_2, LE) fluxes were computed using Eddy-pro 5.1.1 software (www.licor.com), and synchronized with the mean 30-min meteorological parameters from the data logger.

Table 2.1. Study sites description. Basic information regarding the four study sites across the Israeli climatic Gradient

Site	**Yatir**	**Eshtaol**	**Birya**	**Solelim**
Climate	Semi –arid (SA)	Mediterranean (M)	Humid Mediterranean (HM)	Mediterranean
Latitude coordinate	31° 20' 49.20" N	31° 47' 34.50" N	33° 00' 00.50" N	32° 44' 47.00" N
Longitude coordinate	35° 03' 07.20" E	35° 00' 11.50" E	35° 30' 40.50" E	35° 13' 55.70" E
Mean long term annual rainfall (mm)	285	543	755	580
Daily mean temperature (C°)	18	19	17	21
Elevation (m)	650	380	755	190
Forest ecosystem *(dominant species)*	**Pine** forest plantation (*Pinus halepensis*)	**Pine** forest plantation (*Pinus halepensis*)	**Pine** forest plantation (*Pinus halepensis*)	**Oak** native forest (*Quercus calliprinos* & *Q.ithaburensis)*
Trees age (y)	45	46	36	~ 70
Forest density (t h^{-1})	350	480	600	280
Canopy height (m)	10	11	11	8
Soil type	Light brown Rendzina	Light brown Rendzina	Rendzina and Terra rossa	Rendzina and Terra rossa
Non- forest ecosystem	Grass under heavy grazing	Mixed shrubs (annual vegetation)	Grass under heavy grazing	-

The EC system housed on the pneumatic mast (see Fig. 2.2) was positioned in the center of each field site with location and height aimed to provide sufficient 'fetch' (sufficient spatial scale of

uniform ecosystem canopy subject to measurements (roughly, 200-500 meters for a mast positioned 2-5 m above the vegetation canopy). Power was provided by 11 VA generator that was placed about 30 downwind from the mast, and the Mobile lab, detached from the mast, was also positioned about 30 m from the mast to avoid effects on the flux measurements. The system was left unattended during most of the campaign duration, but was supervised by cellular communication to the home lab in the Weizmann campus.

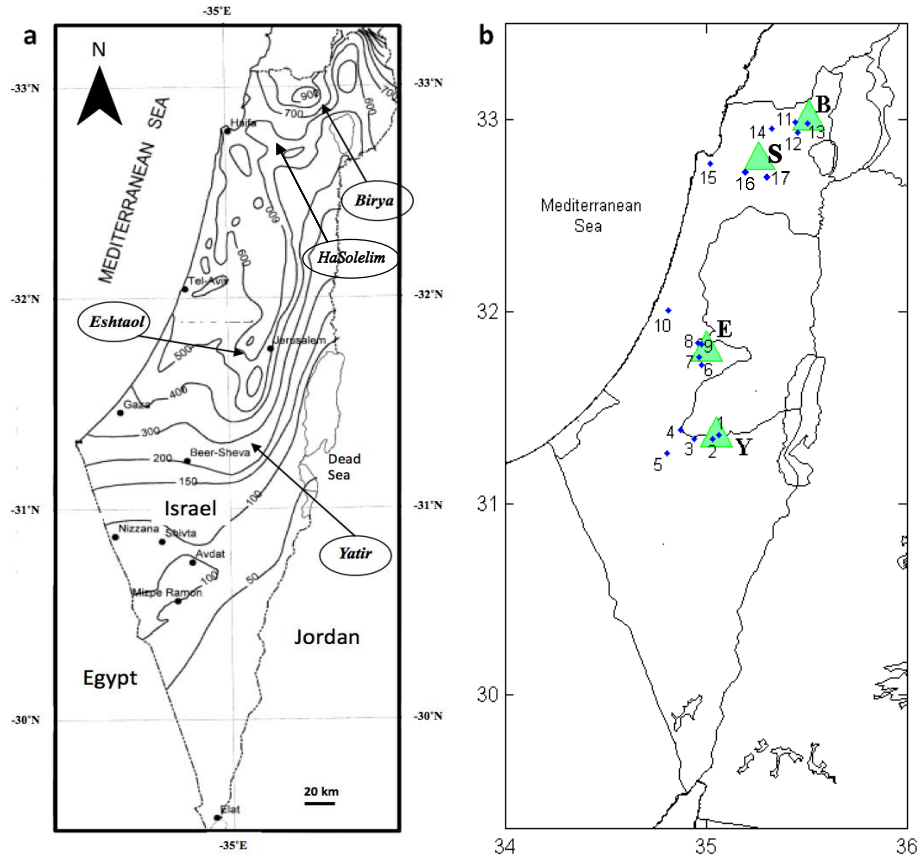

Fig. 2.1. Four study sites and their adjacent meteorological stations along the Israeli Climatic Gradient (ICG). (a) Contour map of mean precipitation (left) with the four study sites (circles): 3 Alepo pine forests, Birya (north), Eshtaol (center), and Yatir (south), and one Oak forest, (intermediate). (**b)** Fifteen meteorological stations (IMS-Israeli Meteorological Services; blue dots) distributed around the study sites (green triangles) were used including: Yatir (1), Shani (2), Meitar (3), Lahav (4), and Ben-Gurion University (5) around Yatir site; Beit Jamal (6), Zora (7), Nahshon (8), Latrun (9),and Beit Dagan (10) around Eshtaol site; Meron (11), Amirim (12), Sefat (13), Harashim (14), and Haifa (Technion) around Birya (B); Neve Ya'ar (15), and Iksal (16) near the Solelim site (S). The distance between the southern and northern sites is about 180 Km.

3.3 Eddy covariance methodology

The EC method for measuring exchanges of heat, mass, and momentum between a flat, horizontally homogeneous surface and the overlying atmosphere was proposed by Montgomery (1948), Swinbank (1951), and Obukhov and Yaglom (1959). Under these conditions, net transport between the surface and atmosphere is one-dimensional and the vertical flux density can be calculated by the covariance between turbulent fluctuations of the vertical wind and the quantity of interest (Foken *et al.*, 2004). The latent heat flux (LE) was calculated by the covariance between fluctuations of vertical air velocity *w (m/sec)*, and water vapor density *q (kg/m3)*, using the formula (Rosenberg *et al.*, 1983):

$$\mathrm{LE} = \rho \mathrm{L_V} \overline{\mathrm{w'q'}} \qquad (4)$$

where ρ is air density (Kg/m3) of wet air, $\mathrm{L_V}$ is the latent heat of water vaporization (2.45 [MJ kg^{-1}]), tags indicate turbulent variance around the mean of a given variable, and the overbar indicate mean values (usually over 30 min) of the high frequency measurements (20 Hz). Other fluxes could be calculated in a similar way, replacing q with H, CO_2, ozone concentrations etc. The logic underlying this model is based on the assumptions that over a uniform horizontal surface, the mean vertical flow ($\overline{w}$) is negligible (no vertical wind is produced or consumed by the surface) and so are also changes in air density during the measurement. However, the variance is composed of turbulent wind eddies that either go up or down and contain different concentration of a given scalar (say, water vapor). Thus, the mean product of the 'variance' of the scalar (q') and that of the vertical wind integrated over the same time is non-zero. This mean 'co-variance' ($\overline{\mathrm{w'q'}}$) gives the net transport of the scalar across the mixed surface layer.

The EC technique is widely used in recent years and allows direct measurements of whole canopy CO_2, H_2O, sensible heat, and latent heat fluxes in different ecosystems, including forest, grassland, desert, and open fields (Beer *et al.*, 2010). The method is based on the assumption that in the mixed surface layer above a canopy surface vertical fluxes of scalars such as water vapor, are approximately constant with the surface layer height. Thus, the flux measured by a sensor at some point well above the canopy but within the mixed surface layer is equal to the flux released or absorbed at the surface. Adequate application of the EC technique requires the validity of the following additional assumptions: the mean vertical air velocity is zero (requiring

the terrain to be horizontal and no losses due to horizontal advections), the land cover is homogeneous, and sufficient "fetch" is available upstream of the measurement point. The 'fetch' requirement is roughly estimated as the uniform surface distance over which the mixed surface layer is formed. Usually (depending on vegetation characteristics, to be in the surface mixed layer, a sensor must be at least 2 m above the canopy surface, which requires a 'fetch' of 200 m (sensor height is ~1% of required 'fetch') of the sensor height. If larger 'fetch' is available, the sensor can be raised in the same proportion and measurements would represent a larger canopy area).

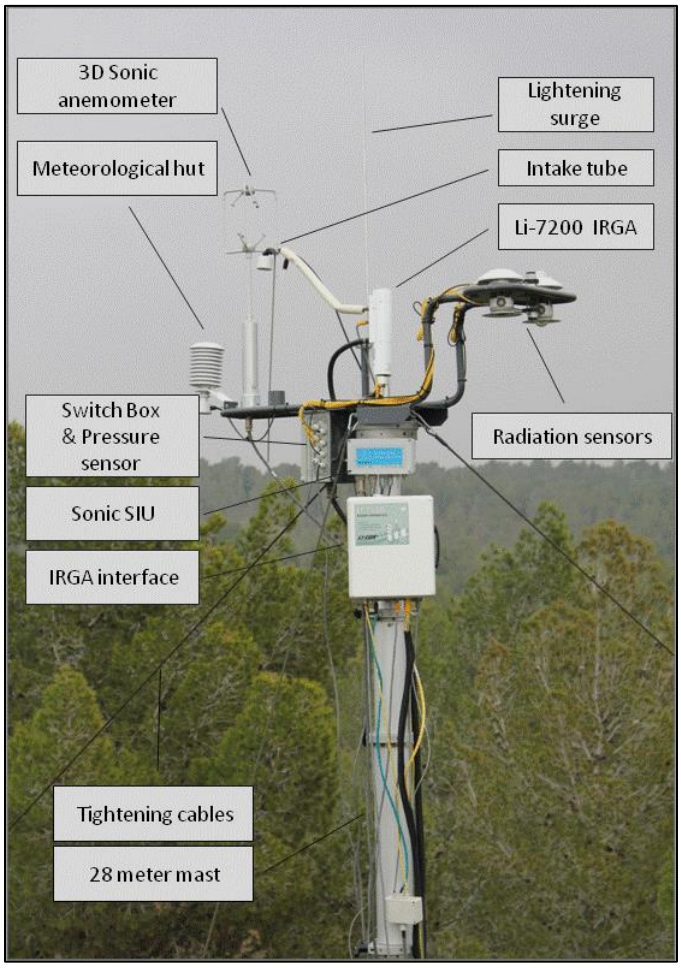

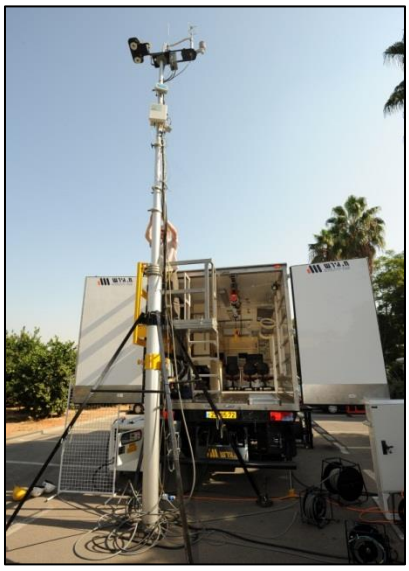

Fig. 2.2. Measurement mobile system. Measuring components (left) installed on top of the mast: Sonic 3D anemometer, Li-7200 IRGA, six radiation sensors (PAR, long and short wave, up and down) and meteorological hut (air temperature and humidity). The mast opened next to the mobile lab (right bottom).

Using high frequency response sensors, measurements of turbulent fluctuations of vertical velocity and scalar concentration can be performed and their covariance, which represents the vertical turbulent flux, can be calculated. The latent heat flux (*LE,* Eq.4*)*, or the equivalent water vapor flux, which are in the center of the current study, were calculated by the covariance

between fluctuations of vertical air velocity and water vapor density. As data are collected at high frequency and continuously, and a series of corrections are required, for example to account for contribution of non-vertical wind contributions, losses of high frequency data, transport in tubing to the analyzers, etc., available software that automate these calculations are used. In this study, we used the state of the art Eddypro software (LiCor, Lincoln, Nebraska).

Table 2.2. Campaigns schedule across the ICG (Israeli Climatic Gradient). Mobile campaigns were conducted during 2012-2015, in three pine forested (F) sites and their adjacent non-forested (NF) sites, located at: Birya (Humid Mediterranean; HM), Eshtaol (Mediterranean; M), Yatir (Semi-Arid; SA), and one native oak forest site, Ha'solelim (M). Each site includes different campaigns in the F (solid cycles), and NF sites (empty cycles). Campaigns were conducted among all three seasons, winter, spring, and summer, in all sites. One campaign, at the non-forested Yatir site, was conducted after the 4 years of measurements during Feb-2016.

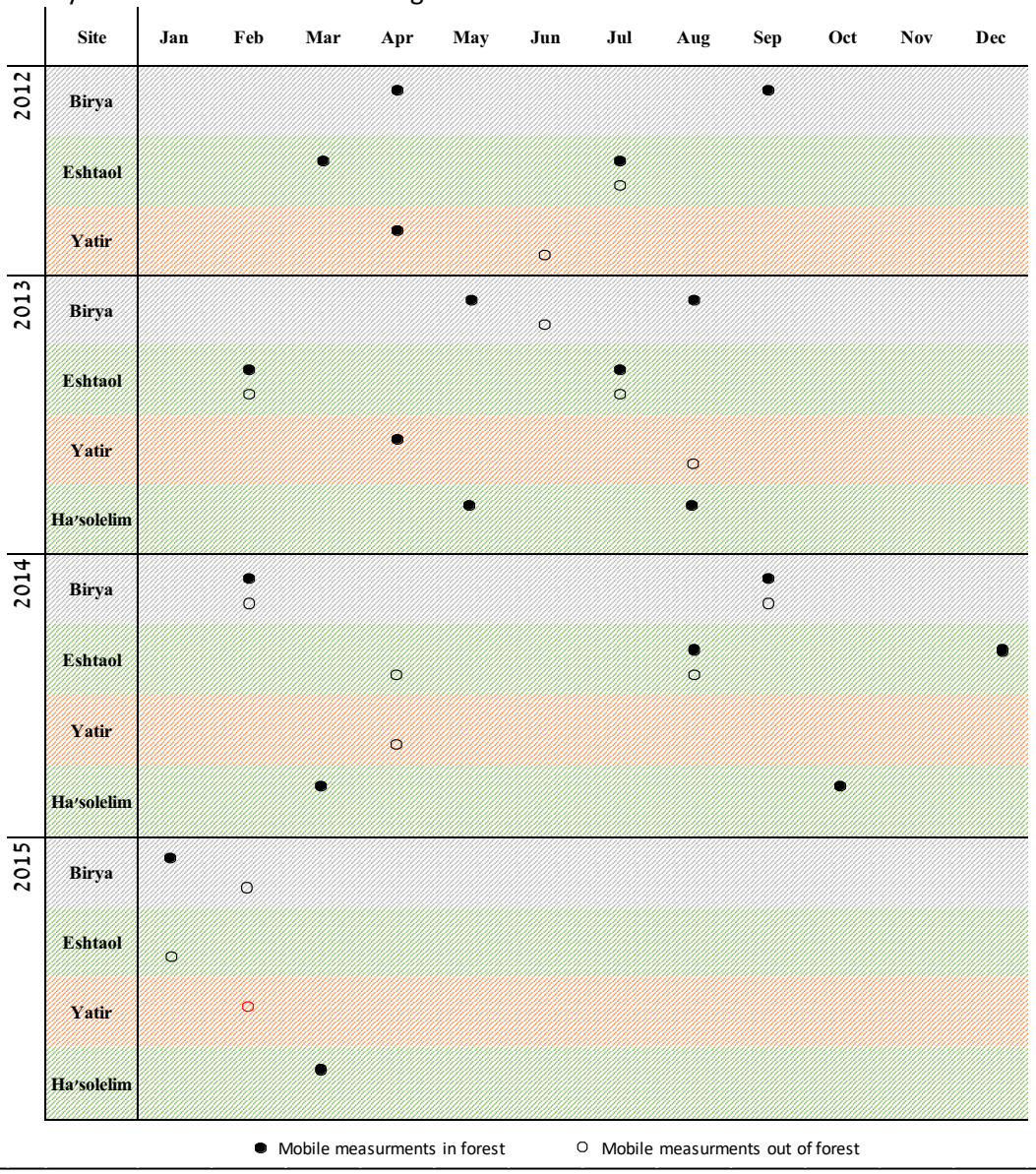

3.4 Data processing

3.4.1 Energy closure constrain

Verification of the flux measurements can be conducted by the energy balance closure analysis (Wilson *et al.*, 2002). Considering a control volume of the measurement system, the 1st law of thermodynamics (law of energy conservation) at steady state (i.e., neglecting energy storage) shows that the net radiation (R_n) input should be balanced by the sum of the output fluxes of soil heat flux (G), sensible heat flux (H) and latent heat flux (LE) following the equation:

$$LE + H + G = R_n \quad (5)$$

To carry out the balance test, the net fluxes measured by the EC technique, are complemented by additional measurements of net radiation and soil heat flux. If the energy balance of the system (Eq.4) is perfectly closed, the flux measurements of H and LE are validated. Hence, incomplete energy closure often observed in field measurements has become a widely investigated issue. Study by (Wilson *et al.*, 2002) showed an average energy balance (EB) deficit of 21% over 22 Fluxnet sites.The systematic closure problem in the surface energy budget has been reported to reach values of up to 40% of R_n (net radiation) over wheat and grassland (Schwiebus and Berger, 2005; Twine *et al.*, 2000). Among other factors, the possible contribution of non-turbulent heat and vapour transport (mean vertical wind $\neq 0$) and spectral losses due to insufficient fetch are possible sources of error. Energy budget must also be considered on sufficient time scale over which the fluxes are expected to balance out and storage terms are negligible, and is often carried out on the annual time-scale. However, in the present study, which was based on short-term campaigns, the energy closure was used as a preliminary quality control tool, and the calculation was implemented (data points of 30 min averages) neglecting the heat soil flux component which is assumed to be negligible and near zero over the 24 hours cycle in our system (i.e. energy budget reduced to LE + H = Rn).

3.4.2 Data quality control

In addition to the energy closure test discussed above, several other quality control steps were performed by the EC software used here (EddyPro program version 5.1.1, LiCor, Lincoln, Nebraska). This included spike removal procedure, performed ("De-spiking and Raw Data Statistical Screening"); manual exceptional outlier spikes removal (for H, LE and CO2 fluxes); and missing flux values (30 min average) were "gap-filling" by a linear fit to available data before and after the gap (missing data was due to technical failure or non-turbulent conditions).

3.5 Meteorological data from the Israeli Meteorological Services (IMS)

Meteorological stations (standard met stations maintained by the IMS, https://ims.data.gov.il/, Fig. 2.1) adjacent to the selected field sites (north, center, and south) were used to obtain information about background meteorological parameters, such as precipitation (P), temperature (T), relative humidity (RH), and global radiation (Rg). =Data from active IMS stations was obtained for the period of this study (2012-2015) as daily mean values, except for P, which was obtained as accumulated daily rain. When more than a single station dataset were available in the vicinity of the field site, data from all available stations were obtained and averaged.

In addition, data sets for same meteorological parameters were obtained from the IMS station for the entire existing record, which was in most cases covering the period 2000-2015. The daily, monthly and annual mean values for T, RH, and Rg for each day of year (365 daily values) were calculated using statistical analysis software (SAS). Precipitation data were processed in a similar way for the last 50 years of available records, separately for the last 10-15 years, depending on the available data, and last 4 years, using accumulated monthly rain.

3.6 Tree sap flow measurements within the forested sites

Rate of water flow in the xylem tissue in tree trunks was measured as "sap flow" (SF). SF was measured continuously since 2009 in sixteen trees in the Yatir forest research site, using lab manufactured thermal dissipation sensors (Granier and Loustau 1994) calibrated with commercial heat balance sensors (EMS, Brno, Czech Republic; Cermak *et al.* 2004). In Birya, Eshtaol and Ha'solelim forests sites, SF was measured over the seasonal campaigns, using trunk heat balance method, THB (Cermak *et al.* 2004). Measurements were taken every 30 s and the 30 min average was saved on a local CR1000 data-logger (Campbell Scientific Inc., Utah, USA). SF rates (kg hr^{-1}) were calculated in relation to the minimum sap flux during the day, as shown in the empirical equation of Granier and Loustau (1994), modified by Kaneti (2010):

$$SF = LCF \times CF \times 0.04284 \times [(\Delta T_{max} - \Delta T_r)/ \Delta T_r]^{1.231} \quad (6)$$

Where SF is the half hourly sap flow rate; LCF is the length compensation factor due to the inability of the 2 cm probes to capture the entire active sapwood depth (estimated to be ~65% for *P. halepensis* in semi-arid conditions; Cohen *et al.* 2008) and was calculated specifically for individual tree; CF is a 'calibration factor' of 2.5 (Steppe *et al.* 2010; Kaneti, 2010); ΔT_r is the

average half hourly temperature difference between heated and non-heated probes, and ΔT_{max} the maximum temperature difference measured during the day (assumed to represent zero sap flow rate). To account for differences among trees and sites, and to allow up-scaling from tree to forest scale, a diurnal sap flux density was calculated:

$$SFD = \Sigma(SF) / Asw \times 1000 \quad (7)$$

Where SFD is the diurnal sap flux density ($cm^3\ cm^{-2}\ d^{-1}$) and Asw is the sapwood area of each individual tree. The summation in Eq. (6) was applied to all measured data points within a day. For the seasonal campaign basis sites, a multi-channel battery-operated measuring system, of the THB method, was used from Environmental Measuring Systems (EMS), Turistická 5, 62000 Brno, Czech Republic (http://www.emsbrno.cz). This method calculates the heat balance of a defined heated space (for detailed information see Cermak *et al.* 2014). Basically, the input energy has to be split between the conductive heat losses and the warming of water passing through, according to the following simple equation:

$$P = SF \times \Delta T \times c_w + \Delta T \times \lambda \quad (8)$$

Where P is the heat input power (W), SF is the sap flow rate ($kg\ s^{-1}$), ΔT is the temperature difference in the measuring point (K), c_w is the specific heat of water ($J\ kg^{-1}\ K^{-1}$) and λ is the coefficient of heat losses from the measuring point ($W\ K^{-1}$).

In the Yatir site where long term high resolution data sets were available, the average sap flux density was up-scaled from tree to forest using the following equation:

$$T_{SF} = SFD \times sd \times Asw \times 10^{-6} \quad (9)$$

Where Tt is the canopy-scale tree transpiration ($mm\ hr^{-1}$), sd is the stand density (300 trees ha^{-1} in Yatir), and Asw is the average sapwood area of the individual trees (158 cm^2).
In the seasonal campaign basis (Eshtaol and Birya forest sites), up scaling of the tree level measurements were done using a linear dependence of tree SF on tree diameter at breast height (DBH) and calculating T_{SF} using predicted SF by DBH classes and stand DBH distribution (Cermak *et al.*, 2004).

3.7 Leaf scale gas exchange measurements within the forested sites

Intensive one-day gas exchange measurements campaigns for each of the seasonal campaigns was performed in the forested sites using leaf gas exchange system Li6400XT (LiCor, Lincoln, Nebraska). Leaf level transpiration rates (T_l) and stomatal conductance (g_s) were measured

between 6:00 a.m. and 6:00 p.m., at a quantum flux density of following sun light diurnal changes measured out of the chamber, and a constant air temperature, during the dry season, of 30 ± 1.5˚C under a controlled CO_2 concentration of 400 ± 2 ppm provided by the gas exchange system.

Representative, 6 pairs of needles from the current year (pine trees) were selected in both sunlit and shaded parts of the canopy, and enclosed in a clamp-on gas-exchange cuvette of 6 cm^2 and 80 cm^3. Airflow through the dynamic cuvette was 500 ml min^{-1}. Rate of net assimilation and leaf transpiration, were calculated based on the chamber flow rate, leaf area (determined by leaf scan and Image-J program), and concentration measurements of water vapor and CO_2 in the inlet and outlet air. Leaf stomatal conductance was estimated from the leaf transpiration rate and water vapor concentration gradient, relying on the chamber measurements and saturation vapor pressure at the leaf temperature according to Von Caemmerer and Farquhar (1981). Leaf temperature was estimated based on leaf energy budget method according to Ehleringer (2000).

3.8 Partitioning of ET and ozone total fluxes to its stomatal flux

In this study, we partitioned simultaneously measured ozone and water flux to its stomatal and non-stomatal component. Concurrently using the partitioning of both gases provides better insight into the different factors and mechanisms that control the water partitioning. The method that was used here for ozone and water partitioning is presented in detail in Lamaud *et. al.* (2009). The method is based on the evaluation of stomatal conductance to water on the canopy scale (g_w) from the total flux. First, surface resistance (R_s) was calculated by Eq. 10 based on a derivation of the Penman Monteith equation for evapotranspiration:

$$ET = \frac{VPD}{R_a+R_b+R_s} \cdot \frac{\rho C_p}{\lambda \gamma} \qquad (10)$$

Where the evapotranspiration flux (ET) is calculated by atmospheric vapor pressure deficit (VPD, Pa), the sum of resistances between plants and atmosphere: air resistance within the inertial sublayer (R_a, m s^{-1}), roughness sublayer resistance (R_b, m s^{-1}), and surface resistance (R_s, m s^{-1}), including stomatal and non-stomatal resistances. ρ is the air density (kg m^{-3}), C_p is the heat capacity for a constant pressure (1005 J K^{-1} kg^{-1}), λ is latent heat of vaporization (2.5x10^6 J kg^{-1}), and γ is the psychometry constant (67 Pa K^{-1}). R_s was then isolated and calculated from eq. 10,

by using EC measurements for ET and VPD parameters, while all other parameters were calculated from known physical equations and climatic parameters measured at the site. Second, the linear regression of surface conductance; G_s ($1/R_s$) over gross primary production (GPP) was obtained. This was done only for relatively dry conditions, characterized by $RH<RH_{thresh}$, where RH_{thresh} is determined by using the highest regression coefficient of the linear regression between G_s versus GPP under different RH values:

$$G_s=a(GPP)+b)) \quad (11)$$

GPP was calculated using net ecosystem exchange (NEE) from the EC method and a conventional approach of estimating ecosystem Re (for more details see Reichstein *et al.*, 2005, Asaf *et al.*, 2013). It is assumed that under dry enough conditions (low RH) the slope (a) of the linear regression equation (Eq. 11) represents the relationship between g_w (stomatal conductance to water) and GPP, while other evaporation components from the surface are negligible (such as soil evaporation), and are represented by b in Eq. 11. Using the derived relationship between (a) and GPP, g_w can then be calculated also for RH> RHthresh.

Stomatal ozone flux (F_{O3sto}) was then calculated using the ratio between diffusivity coefficients of water and ozone, and ozone atmospheric concentration nearby the leaf (by using atmospheric resistances as described by Gerosa *et al.*, 2005). Finally, the transpiration flux (T_{gw}) was up-scaled from g_w using Eq. 3 (see chapter 1.4 for more details). When Eq. 3 is used for the calculation of transpiration rates, VPD should refer to the leaf scale (delta-E), representing the difference between air and leaf actual vapor pressure. For this to be achieved the correlation between VPD from atmosphere EC measurements and delta-E from leaf scale LI6400 measurements was used (Klein *et al.*, 2015). Improvement to this methodology was achieved by finding the relationship between delta-E and VPD, according the time during the day, which can be used as a first approximation parameterization for the impact of atmospheric stability on the relationship between the two.

4 Results

4.1 Israel climatic gradient

4.1.1 Inter-annual variations in climatic parameter across Israel

This study focuses on the effects of the Israel climatic gradient (ICG) on ecosystem water balance, and the parameters of it is composed. Here the climatic gradient was examined based on four major parameters: precipitation (P), temperature (Ta), global radiation (Rg), and vapor pressure deficit (VPD). Data measured at 3-4 meteorological (Met) stations which were the nearest to each study site were obtained from the Israeli Meteorological Services (IMS, Beit-Dagan, Israel, Fig. 2.2). The climatic gradient of Israel is described here by changes of climatic conditions in three sites, from semi-arid (SA) to Mediterranean (M) and humid Mediterranean (HM) climates (Fig 3.1a-d). Annual means were averaged for 15 hydrological years, 2000/01-2014/15, and for 4 hydrological years, 2011/12- 2014/15, during which measurements along the gradient were taken in the framework of this study (Hydrological year was defined from 1st of October, assuming no major rain events occurred before, to 30th September). In the M sites data were available only since 2004 allowing averaging of 10 years only. P and T were significantly different between the 3 climatic sites along the gradient (Tukey HSD, $P<0.001$), with increasing P, from 284 mm yr^{-1} at the SA site, to 479 mm yr^{-1} at the M site, and to 766 mm yr^{-1} at the HM site (Fig 1a). Ta differed significantly among sites (Tukey HSD, $P<0.001$), with the lower altitude M site (see table 2.1) showing consistently higher Ta than both the HM and SA sites, and the SA site showing higher Ta than the HM site (Fig 3.1c). VPD showed a decreasing trend from the SA to the HM site in the 4-years observation period but not in the 15-year observation where the low altitude M site showed high VPD values similar to the SA site. VPD was significantly lower in the HM site when comparing to the M site, but did not differ significantly between the M and SA sites (Fig 3.1d). Rg was significantly higher in the SA site when compared to the other sites (probably due to lower cloud cover), but did not differ significantly between the M and HM sites (Fig 3.1b). When comparing the two periods examined, 15 and 4 hydrological years, it seems that while for P, Rg and Ta, the last 4 years of measurements are well representative of the last 15 years in all 3 sites, VPD was more fluctuating, with no clear gradient pattern in both periods.

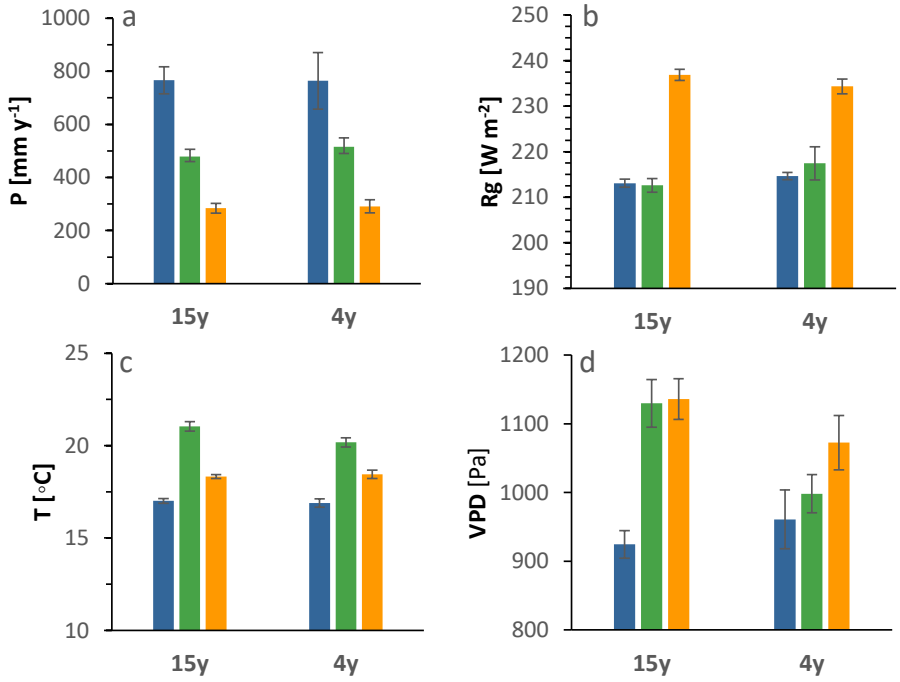

Fig.3.1.The multi-years annual means of meteorological parameters along the Israel Climatic Gradient (ICG) from three Aleppo pine forest sites during 2000-2015. Meteorological data was provided by the Israel Meteorological Services (IMS) using the measurement stations around the sites of interest; Humid Mediterranean (**HM**, blue columns), Mediterranean (**M**, green columns), and Semi-Arid (**SA**, orange columns). The colored bars are for 15 and 4 hydrological years averages of a- precipitation (**P**), b- global radiation (**Rg**), c- air temperature (**Ta**), and d- vapor pressure deficit (**VPD**). Error bars represent the standard error of mean (n=15, n=4).

4.1.2 Precipitation anomalies

Although the slope of increasing P along the ICG is consistent almost across all years (Fig. 3.1a), considerable inter-annual variations are observed in the annual precipitation data. The magnitude of the inter-annual fluctuations, however, are not the same in the three sites. This can be seen in the standard deviation (SD) of P in the different sites, which correlate well with the mean site P, higher annual mean of P is associated with higher SD of P (SD = ±202, ±146, ±92, for the SA, M and HM sites, respectively, R^2=0.996).

This is highlighted also by the inter-annual anomalies of P (Fig. 3.2). Differences in inter-annual variability of P can be an important factor in the ecosystem water cycle, and the ability of plants to adapt to changing environments and should be take into account in comparing activities in

the different sites. When comparing the relative variations in P among sites (SD/P), the variations in P increased from ±27% in the wet site to ±31% in the dry site. The differences in inter-annual variations are more expressed during the 4 years of measurements (Fig 3.2 insert), with wide range of annual P in the HM site, from 450 to 885 mm yr^{-1}, and more moderate inter-annual variations in the M and SA sites, from 495 to 654 mm yr^{-1}, and from 249 to 358 mm yr^{-1}, respectively.

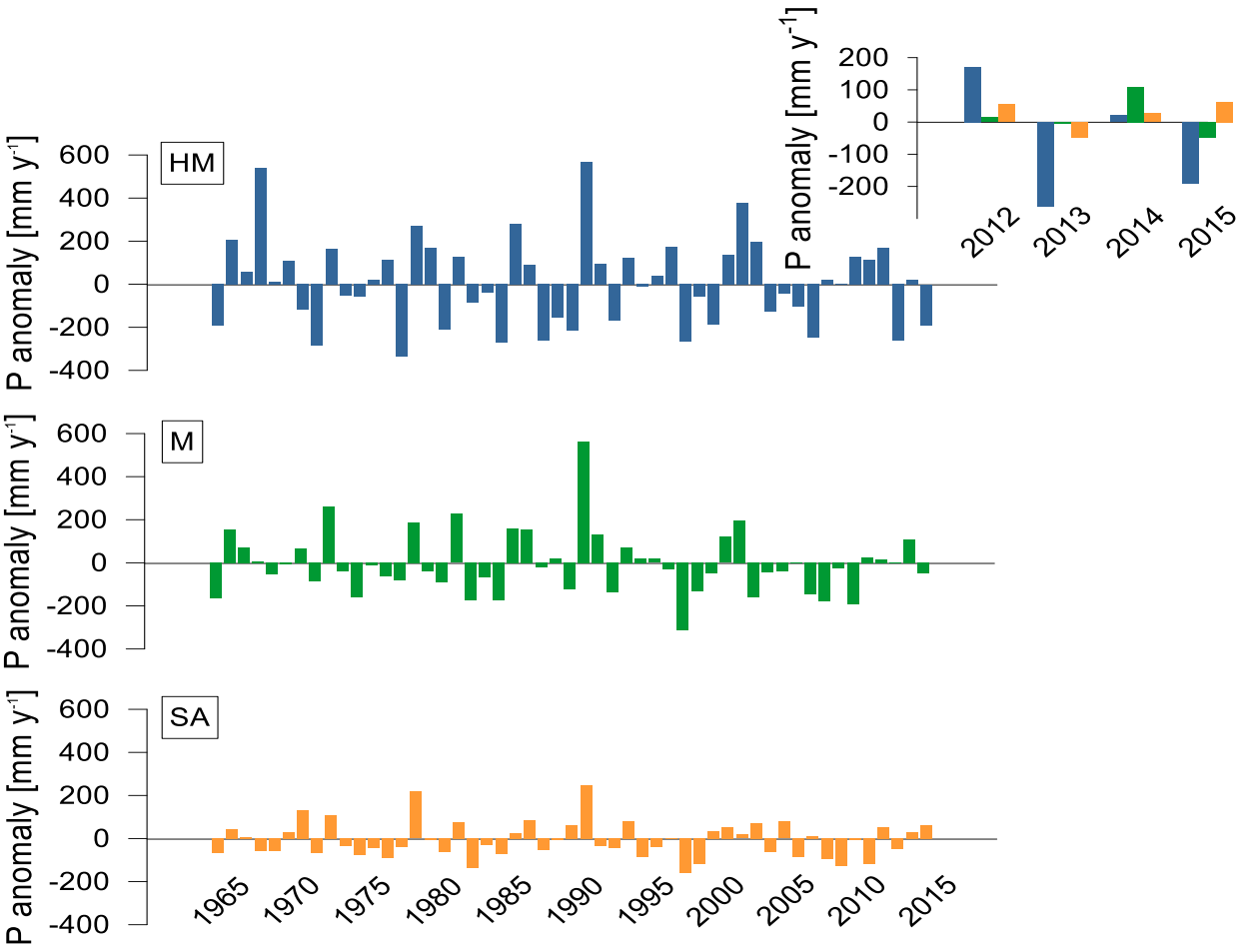

Figure 3.2 Precipitation anomalies along the ICG sites during 1965-2015. The 50y's precipitation means, HM (Blue), M (Green), and SA (Orange), are: 751±202, 544±146, 295 ± 92 mm (means±SD) respectively. The Insert focuses on P anomalies during 4 years of measurements, 2012-2015.

4.2 Estimating continuous ET from the Flux Meteorological Algorithm (FMA)

One of the objectives of this research was to use the short campaign measurements as an observational basis to produce continuous, seasonal, and inter-annual scale dataset of ecosystem fluxes across the ICG and in different vegetation types. This was based on the

following steps that described our approach to meteorologically based flux estimates (Flux Meteorological Algorithm; FMA):

Step 1: Adjusting IMS meteorological parameters to the measurements site

Step 2: Obtaining correlation equetions between measured ecosystem fluxes and climatic virables

Step 3: Estimating continuous ecosystem fluxes combining steps 1&2

For Step 1 we correlated the daily mean values of the climatic parameters during the measurements periods with the long-term mean values for each site (averaged by day of year), for each site and climatic parameter (Rg, Ta, and VPD; Fig. 3.3). Soil water content and wind speed where missing parameters from the IMS nearby stations and therefore where not included in the analysis. Note that on average ~ 70% of the measurements days were within the

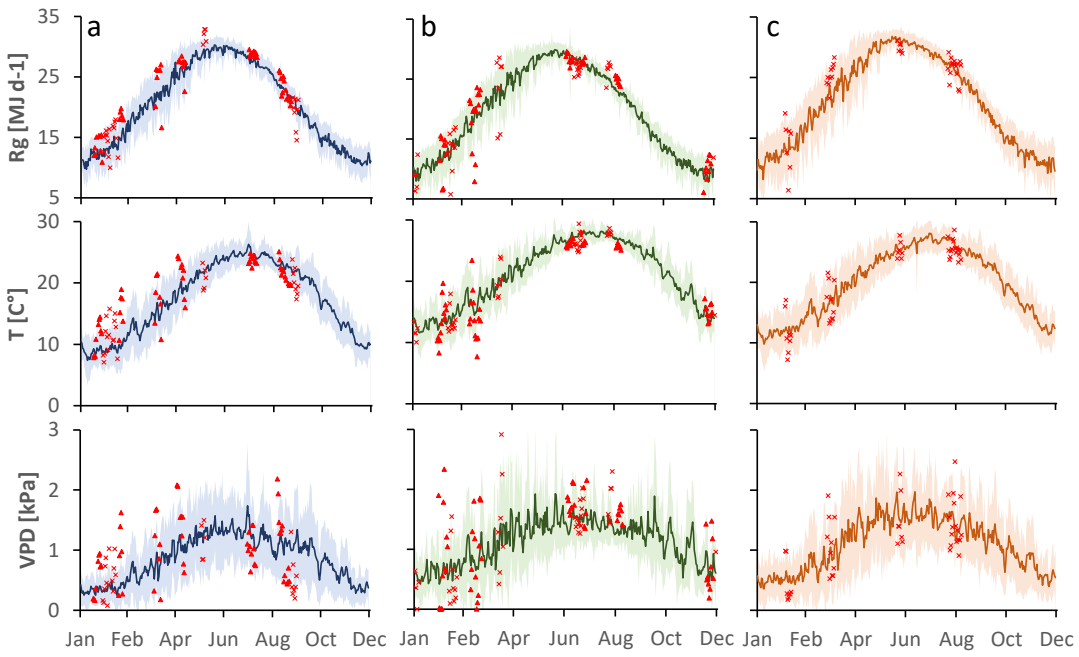

Figure 3.3 Seasonal cycle of daily global radiation (Rg) mean daily temperature (T) and mean daily vapor pressure deficit (VPD) along the Israel Climatic Gradient (ICG), Humid Mediterranean (HM; a), Mediterranean (M; b), and Semi-Arid (SA; c). Mean seasonal cycles averaged by day of year (DOY) during 15y (2000-2015) is indicated by the dark solid line. Colored shades indicate standard deviation from the means (SD). Direct observations from the mobile system are indicated by red triangles (forested sites) and red Xes (non-forested sites). On average 70% of the measurement days were within the standard deviation of the long-term mean for all three parameters.

standard deviation range (Mean±SD) of all three parameters, Rg, Ta, and VPD (Fig. 3.3), living only 30% as extreme conditions days, which can be consider as well representatives of the past 10-15 hydrological years. This indicated that the conditions during the campaigns were typical for the site. Some exceptions were observed during hot days in winter campaigns (Jan, Feb) of the HM and M forest sites, when VPD exceeded the SD range in 60% and 67% of the measurements days, respectively.

To quantify possible small differences between values of measured meteorological variables in the mobile-lab or at the IMS stations, due to differences in measurements site characteristics (such as altitude, slope and slope direction, etc.) the correlation between each of the three meteorological parameters (Ta, RH, and Rg, daily mean values) measured at the sites and the respective parameter recorded by the adjacent IMS stations, were determined, using a linear regression (eq. 12).

$$X_{Mbl_{(site)}} = a\,(X_{IMS_{(site)}}) + b \qquad (12)$$

Where, $X_{Mbl_{(site)}}$ and $X_{IMS_{(site)}}$ are the daily mean values of meteorological variable measured by the Mbl and the corresponding variable measured by IMS, a and b are site specific regression coefficients . Regression was performed for all days of mobile system measurement campaigns at any given site (Fig. 3.4). By applying, the linear equations to the IMS data, the 'site adjusted'

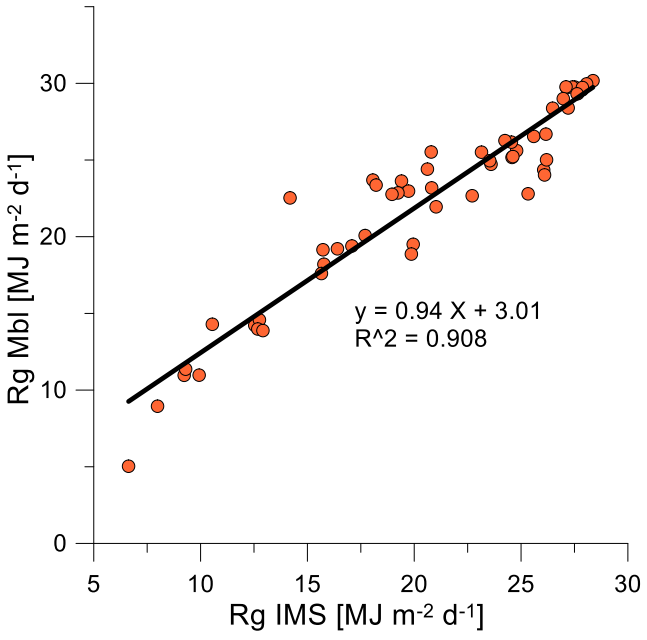

Figure 3.4 Adjustment of the meteorological parameter to the mobile lab site location: Linear regression of global radiation (Rg) measured at the mobile lab (Mbl, y axis) vs. Rg from the adjacent stations of the Israel Meteorological Service (IMS, x axis), as measured in Birya forest and its adjacent IMS stations.

daily means T, RH, and Rg were obtained for the entire period for which IMS data were available for all sites.

In addition, it was found that a 'seasonality index' is needed, especially to adjust the data to the long seasonal drought in our regions. For this, the transpiration deficit (D), was used and was obtained from the cumulated (starting from October 1) difference between precipitation (P) and potential evapotranspiration (PET), the last was calculated by Priestley-Taylor (PT; Priestley & Taylor, 1972). The coefficients for PT were calculated using adjusted IMS climatic variable from Eq. 12, with a specific modification for the alpha coefficient based on its dependent of VPD (for more details see Steiner *et al.,* 1991). It was assumed that D could not fall below zero (when no soil water is available for evaporation) and helped adjusting ecosystem fluxes and activities to the seasonal drought periods. It was calculated as follows:

$$D(t) = \max\left(\left(\sum_{i=t_0}^{t} P(i) - PET(i)\right), 0\right) \quad (13)$$

Where t is the day of hydrological year and t_0 is October 1st (day 1). D was then added to other meteorological parameters for the regression at step 2.

For Step 2, the dependencies between measured variables (ET, H, LE, and Rn) and adjusted meteorological parameters (T, RH, Rg, VPD and D) measured at the mobile sites during our campaigns, was analyzed and best fit equations were acquired. This was achieved by a multiple stepwise regression calculated for the combined dataset of all campaigns in each site (e.g. number of equations equal to number of sites), with the following generic linear equation:

$$y = \mathrm{a} + \Sigma_i b_i x_i \quad (14)$$

Where y is the ecosystem flux of interest, in this specific work ET, a and bi are parameters and x_i are T, RH, Rg, VPD or D. The selection of meteorological variables (x_i) was done by a stepwise regressions of $y(x_i)$, b_i=0 when a specific x_i was eliminated.

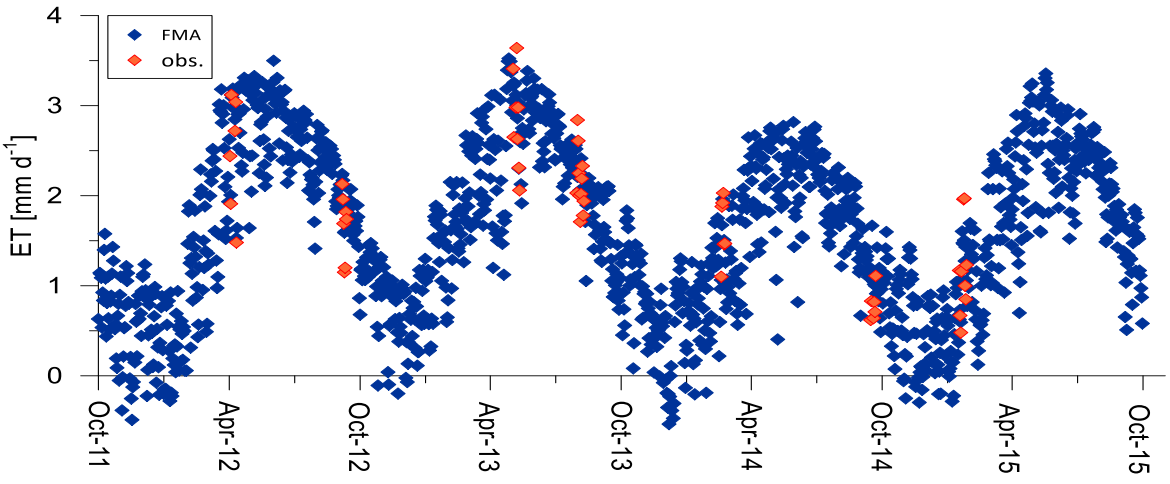

Figure 3.5. Observed and estimated ET: continuous estimated daily ET from the Flux Meteorological Algorithm (FMA, blue closed diamonds) and observed ET (obs., red closed diamonds) by the eddy co-variance mobile lab, during 4 hydrological years of measurements, as calculated and measured in the Humid Mediterranean (HM) forest site. Obs. vs. FMA daily ET gave high correlation, with R^2=0.83.

Finally, for Step 3, we combined the adjusted long-term Met data from IMS station associated with each site of Ta, RH, Rg, and VPD and the stepwise equations abstained above to derive a continuous record of ET, H, LE, and Rn for our study sites. For example, ET in the HM site (Fig. 3.5) was obtained by the following equation (for all equations and FMA results see appendix table A1 and Fig. A1):

$$ET = 0.0928Rg - 0.016RH + 0.0015D + 0.29 \quad (15)$$

In two campaigns (M forest, February 2013 and HM non-forest September 2014) rainy days from the regression were excluded (in the last case also 3 days after rain were excluded). In the case of SA non-forest site, instead of linear regression, a nonlinear one was applied, in the Gaussian form:

$$ET = a \cdot \exp(-\sum_i b_i(x_i - c_i)^2) - y_0 \quad (16)$$

Where a, b_i, c_i and y_0 are parameters and x_i are T, RH, Rg, VPD or D. The selection of meteorological variables (x_i) was done manually by means of analysis of $y(x_i)$ dependences for all x_i variables.

4.3 The effect of land use change on Evapotranspiration and ecosystem Water Yield along the Israel Climatic Gradient.

4.3.1 Seasonal scale changes in ET

We first examined changes in ET along the ICG and between ecosystem types at the seasonal time scale (winter, spring, summer) where a direct comparison of measurements and FMA-based estimates are possible. This also highlights the interactions between the climatic effects associated with the ICG and the strong seasonal changes in our region. However, it also offers the opportunity to assess the FMS-based estimates, before considering the annual scale variations in ET that is possible based on the FMS estimates alone. Four years of short campaigns measurements were summarized into three seasons as follows: winter (Dec-Feb), spring (Mar-May), summer (Jul-Sep). In some sites, exceptions were made due to lack of campaigns in a specific season, (e.g. spring of the NF HM site was included end of May beginning of June). Such adjustments reflect the complexity of the campaign-based research approach used here and will be further considered in Discussion section. Note also that for the SA forest site ET is based on available long-term observations in both the seasonal and annual time scales, and no FMA-estimate were used in this case.

Figure 3.6 examines changes in the average daily ET of each season between F and NF sites, along the ICG, and compares these variations based on the observations (Fig. 3.6a), and those estimated by the FMA approach (Fig. 3.6b). Overall, both methods show similar seasonal trends in ET with highest values in spring compared with both winter (low radiation, VPD and temperature) and summer (low water availability). Both methods also indicate higher ET in F than in NF sites, and similar trends along the ICG, and with the differences between both ecosystems and location along the gradient diminishing in winter.

Specifically, F sites show increase in ET with increasing P along the ICG, from 1.5 to 2.5, mm d^{-1}, in spring, and from 0.7 to 1.7 mm d^{-1}, in summer. In the NF sites this trend is less clear, due to high ET in the low altitude M site in both summer and spring. During winter, differences in ET along the ICG diminish, and no clear trend is observed in both F and NF ecosystems, and using both methods. The ratio of ET_F/ET_{NF} provides a useful indicator for evaluating the agreement between the FMA and the observations. Although the absolute values are not identical, both methods reflect the general trend of increasing ET in the F compared to the NF sites, as could be

expected with the increase in leaf area index. Both methods also indicate increase in the ET_F/ET_{NF} ratios when moving from the wet season (winter) to the dry season (summer), as could be expected due to continued summer activity and more extensive root system in forests. The average ET_F/ET_{NF} ratio of all 3 paired sites increase to a similar extent based on both methods,

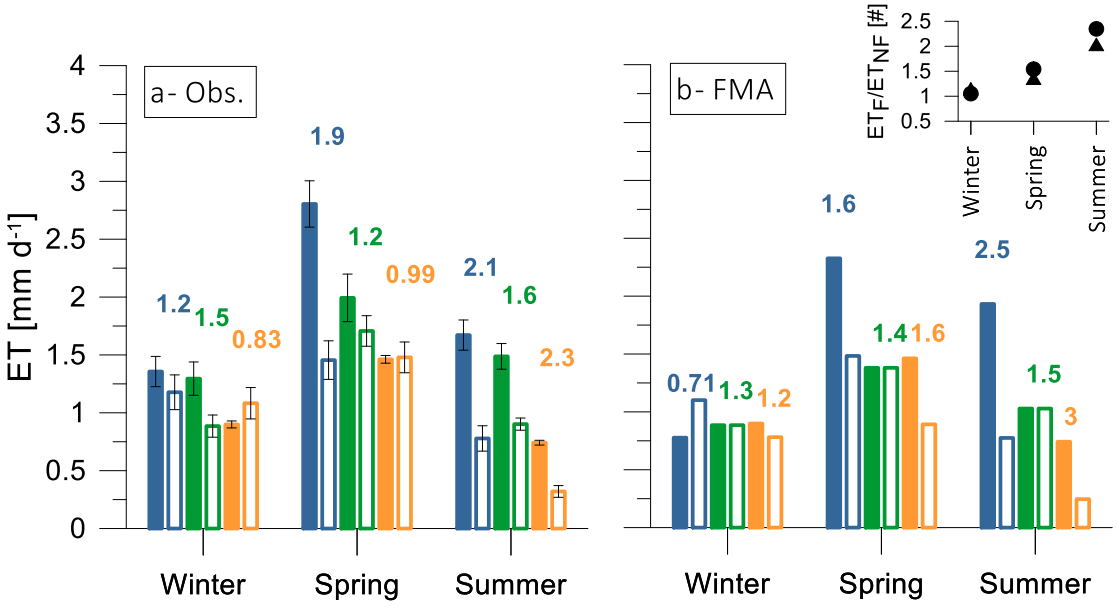

Figure 3.6 Observed (a) and Flux Meteorological algorithm (FMA) estimates (b) daily ET along the ICG for both forested (F) and non-forested (NF) ecosystems in 3 seasons: Winter (Dec-Feb), spring (Mar-May), and summer (Jul-Sep). Full bars are for the F sites, and empty bars are for the NF sites (blue-HM, green-M, and orange-SA). Numbers above each paired bars (F & NF) indicate the ET_F/ET_{NF} ratio per site. Standard error of the mean for measurement days is indicated. Observed ET fluxes were averaged by the 3 seasons periods from the campaign measurements (a). Estimated ET fluxes from the FMA, and from continuous flux measurements during 4 years of measurements, were averaged by the 3 season's periods (b). Insert shows the average ET_F/ET_{NF} ratio of all 3 paired sites in each season and both methods, averaging the observations (closed triangles) and averaging the FMA data (closed cycles).

from 1.1 to 2 and from 1 to 2.3, when shifting from winter to summer in the observation and FMA methods, respectively (Fig. 3.6 insert).

4.3.2 Patterns of the annual ET cycle along the ICG

Using the FMA methodology, ecosystem flux data were extrapolated to the previous 10-15 years (since 2000 in the HM and SA sites, and since 2004 in the M sites) using continuous meteorological parameters from the IMS stations associated with our field sites. To evaluate the mean annual cycle in ET, mean daily ET was obtained by averaging ET values by day of year (DOY) over the entire data set (15 years in the HM and SA sites, and 10 years in the M site).

The results indicated significant shifts in ET seasonality along the climatic gradient, with differential effects on F and NF ecosystems (Fig. 3.7a). In the forested sites peak ET shifted from early March in the dry site to late April in the M site and late May in the HM site. In the NF sites, ET showed similar shifts from late Feb. in the SA site to late March in the HM site, and even larger shift to mid-May in the M site. ET in the SA NF site, showed an unusual small early peak during early winter time (Nov.) which may reflect the contributions of early germination of seasonal annuals.

The differences in ET between the F and NF were smaller during winter (Nov.-Feb.) in all sites, as also observed in the seasonal-scale results presented above. The differences increased during spring and summer, most dramatically in the HM sites, reflecting the mismatch in the ET peak time in the F vs the NF sites (Fig. 3.7b). For example, in the HM site, ET peaked in late March and in late May in the NF and F site, resulting in peak ET-difference in May. These effects were smaller in the other sites.

4.3.3 Annual scale ecosystem water yield (WYe)

Total annual ET values were obtained from the annual sum of daily ET estimated using the FMA approach according to hydrological years (1st of Oct to 30th Sept.). Annual ET values were associated with the corresponding mean annual P values obtained from the nearest IMS stations to each paired field sites along the ICG.

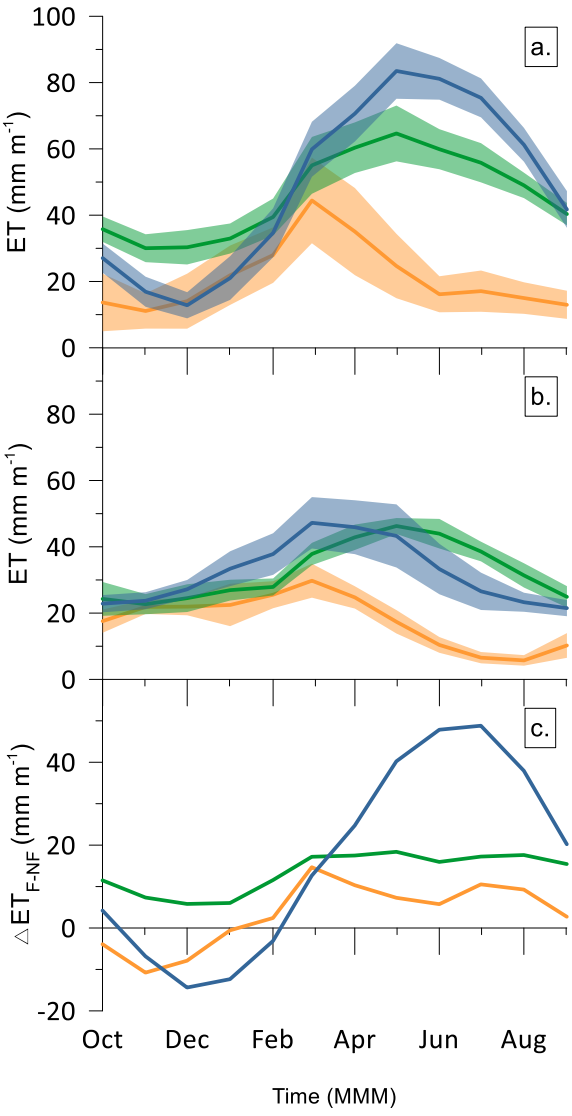

Figure 3.7. Annual cycle of daily ET along the ICG for both Forested (F) and Non-Forested (NF) ecosystems: Continues lines are for the F**(a.)** and NF **(b.)** sites (blue-HM, green-M, and orange-SA). The estimated ET fluxes from the Flux Meteorological Algorithm (FMA) are averaged by day of year (DOY), from continues estimated fluxes during the 10-15 years, and summed for averaged monthly ET in mm per month. **(c.)** Difference between Forest (F) and Non-Forest (NF) ET (ΔET_{F-NF}).Colored shades indicate standard errors for each month (SE).

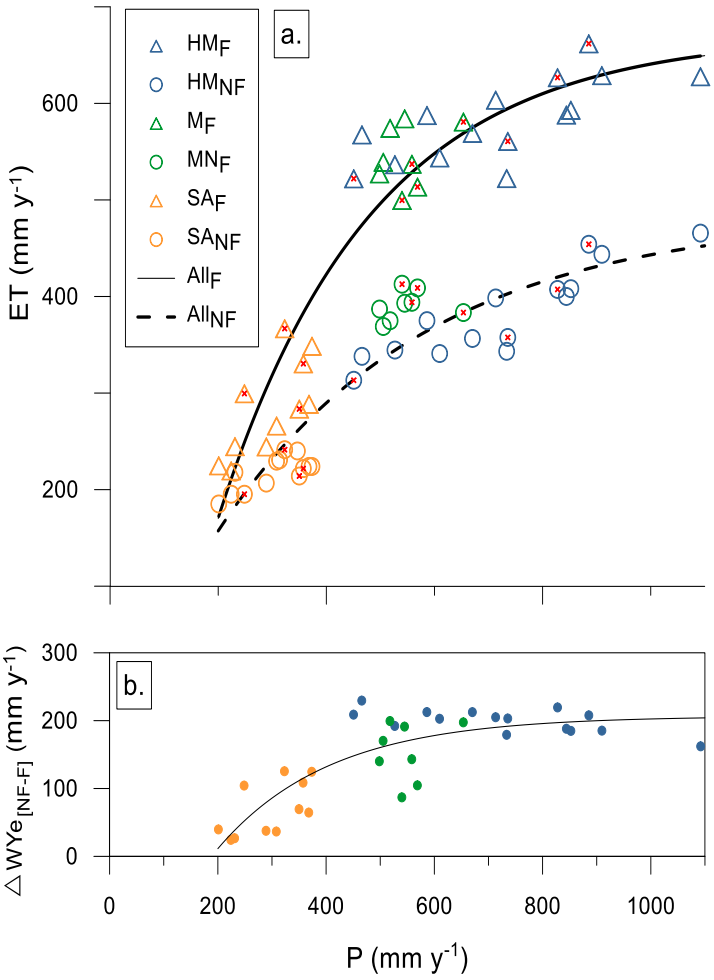

Figure 3.8. Estimated annual sums of Evapotranspiration (ET) vs. annual Precipitation (P) from all sites along the ICG (a): Open triangles are for the F sites, and open cycles are for the NF sites (blue-HM, green-M, and orange-SA), 4 years of measurements time are marked in red X's. The estimated ET fluxes from the Flux Meteorological Algorithm (FMA) are summed over hydrological years (Oct-Sep), from continues estimated fluxes during 2000-2015 (in the HM and SA sites) and during 2004-2015 (in the M sites). Annual precipitation (P) data were collected from the nearest IMS stations. Fitted lines are for the relation between ET and P, for all forested sites (continues black line), and all non-forested sites (dashed black line). Differences between ET in each paired ecosystem types can be represented also as the difference between the ecosystem water yield ($\Delta ET_{F\text{-}NF} = \Delta WY_{e\ F\text{-}NF}$), assuming no differences between the F and NF P in each paired sites **(b)**.

The results showed that ET was generally higher in F sites compared to NF sites, except in the lowest P cases where differences diminished (Fig. 3.8). In addition, in general, ET increased with increasing P along the ICG, but with declining slope (sensitivity) in the ET vs. P relationships at high P values. The ET sensitivity, ET/P, showed a decrease from 94% to 80% in the SA and HM forests respectively and from 76% to 53% in the parallel NF sites (Table 3.1).

Ecosystem water yield (WYe=P-ET, mm yr^{-1}) was generally negatively correlated with ET. Therefore, at the same location and P level along the ICG, forests with higher ET had lower WYe compared to associated NF ecosystems. Assuming negligible differences in annual P between the paired F and NF sites, the difference in annual ET between F to NF can be directly converted into differences in the WYe:

$$\Delta WYe_{[NF\text{-}F]} = (P\text{-}ET_{NF})\text{-}(P\text{-}ET_{F}) = ET_{F}\text{-}ET_{NF} \qquad (15)$$

in each of the paired sites (Fig. 3.8 insert). This indicated that Δ $WYe_{[NF-F]}$ increased with P along the ICG, and within the SA site. At high P level, above about 500 mm, Δ $WYe_{[NF-F]}$ stabilizes and becomes insensitive to P.

The long-term annual sums of ET and P, from the FMA, were averaged for multi-year means of each site in two periods; the 4 years of measurements period (2011/12 until 2014/15), and the 10-15 years of extrapolated data (from 2000/01 in the HM and SA sites, or from 2004/05 in the M sites, until 2014/15 in both cases). The two averaging periods showed high similarity. The 10-15 yrs annual means (Table 3.1) showed that decrease in annual precipitation by a factor of ~2.5, resulted in nearly similar decrease in ET by a factor of 2.2 from 583 mm to 267 mm, and with corresponding change WYe by a factore of about 12, from 144 mm, in the HM forest, to 12 mm, in the SA forest. In the non-forest ecosystems ET showed smaller decrease (by a factor of 1.8) from 383 mm to 216 mm, but with smaller decline in WYe, by a factor of ~5 from 344 mm, to 70 mm. Accordingly, Δ $WYe_{[NF-F]}$ decreased from 200 mm to only 58 mm between the wet and dry conditions.

Table 3.1 Multi-years annual means of water fluxes along the ICG: the presented annual means of the ecosystem water components; Evapotranspiration (ET), and ecosystem Water Yield (WYe) are calculated from the FMA data, annual precipitation (P) was collected from the Israel Meteorology Stations (IMS) nearby stations. All fluxes were averaged for the last 15 and 4 hydrological years in the Humid Mediterranean (HM) and Semi Arid (SA) sites, and 10 and 4 hydrological years in the Mediterranean (M) sites. The difference between non-forest (NF) and forest (F) ecosystem water yield is presented under the title Δ $WYe_{[NF-F]}$.

Site	P [mm y-1]		ET [mm y-1]		WY [mm y-1]		ET/P		Δ $WYe_{[NF-F]}$	
	15y	4y	15y	4y	15y	4y	15y	4y	15y	4y
HM_F	727	725	583	593	144	132	80%	82%	200	210
HM_{NF}	727	725	383	383	344	342	53%	53%		
M_F	548	580	545	533	4	47	99%	92%	154	133
M_{NF}	548	580	390	400	158	180	71%	69%		
SA_F	285	320	267	320	12	0	94%	100%	58	102
SA_{NF}	285	320	216	218	70	102	76%	68%		

4.4 Interactions between environmental conditions and Evapotranspiration (ET)

To examine the interactions between the environmental conditions and ET, in the different ecosystems, we focus on the high resolution diurnal cycles, partitioning of ET to its main components, and consider physiological parameters in addition to climatic factors.

4.4.1 Diurnal cycle of ET

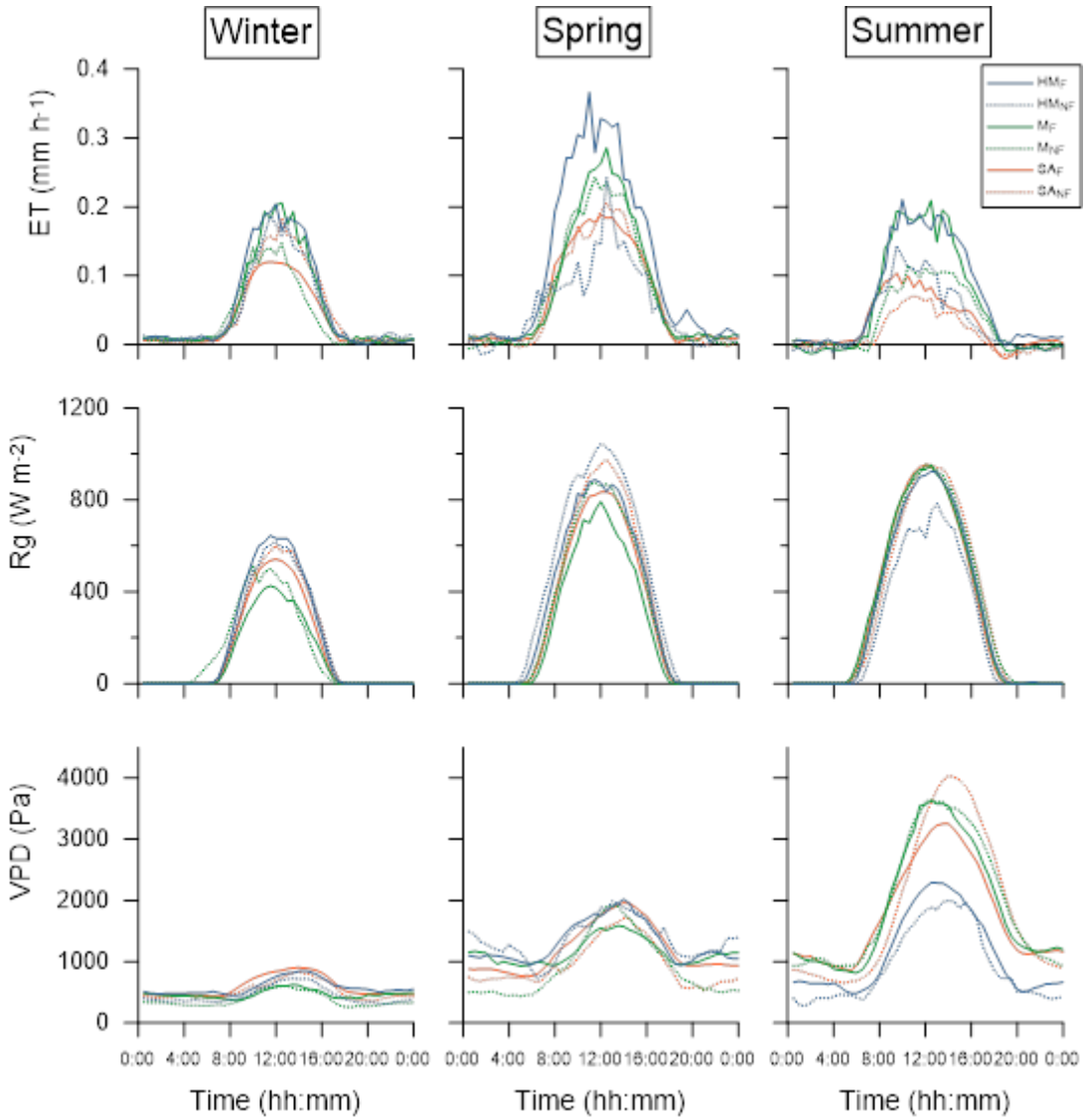

Fig 3.9. Diurnal changes in Evapotranspiration (ET), global radiation (Rg) and vapor pressure deficit (VPD) along the ICG for both forested (F) and non-forested (NF) ecosystems, in 3 seasons: Winter (Dec.-Feb.), spring (Mar.-May), and summer (Jul.-Sep.). Solid lines are for the F sites, and dotted lines are for the NF sites (blue-Humid Mediterranean; HM, green- Mediterranean; M, and orange- Semi-Arid; SA). Parameters are averaged for each hour of the day from campaign basis measurements.

Ecosystem evapotranspiration, which includes plant transpiration and soil evaporation respond mainly to global solar radiation (Rg), and the atmosphere demand to water vapor (VPD)

resulting in the typical diurnal cycles reported in Fig. 3.9 (top panels). ET follows the increase of Rg and VPD from morning until noontime and the decrease in these parameters in the afternoon. Solar radiation (Rg) is not expected to vary significantly across the small spatial scale of the ICG (~180 Km) and the small variations observed probably reflect mainly random variations in cloud cover, during the campaigns, or due to elevation differences (see table . Solar radiation does change significantly along the annual cycle increasing from about 500-600 Wm^{-2} in the winter to around 1000 Wm^{-2} in the late spring and summer. In contrast to Rg, VPD does change significantly across the ICG, which is most prominent in summer when the SA sites have markedly higher VPD values than the wetter sites. VPD also increase along the annual cycle from mid-day values less than 1000 Pa to nearly 2000 Pa in spring and up to 4000 Pa in the SA sites in summer. Differences between ecosystems are also observed and are most prominent in summer in the SA sites, where VPD in the NF site was higher than in the forest site.

The seasonal campaigns showed changes in the characteristics of ET diurnal cycle both along the annual cycle, and along the ICG (Fig. 3.9). These changes must reflect interactions among radiation, VPD, soil moisture, and the plant response (e.g. adjustment of stomatal conductance to soil or atmospheric moisture stress). In general, the results show that lower VPD and Rg during winter time, and therefore lower evaporation demands, are reflected in lower ET, flattened diurnal curve, and smaller differences among sites. When entering the active season (spring time) both VPD and Rg increases, resulting in a parallel increase in ET fluxes reach their highest annual values, with sharper mid-day peak and clearer differences between ecosystems in the HM and M site, compared with the SA sites. The highest ET differences between ecosystems and sites are expressed in the dry season (summer time), associated also with a shift to earlier peak of ET, most apparent in the SA sites and non-forested HM site, compared with the more flattened peak in the M and forested HM sites.

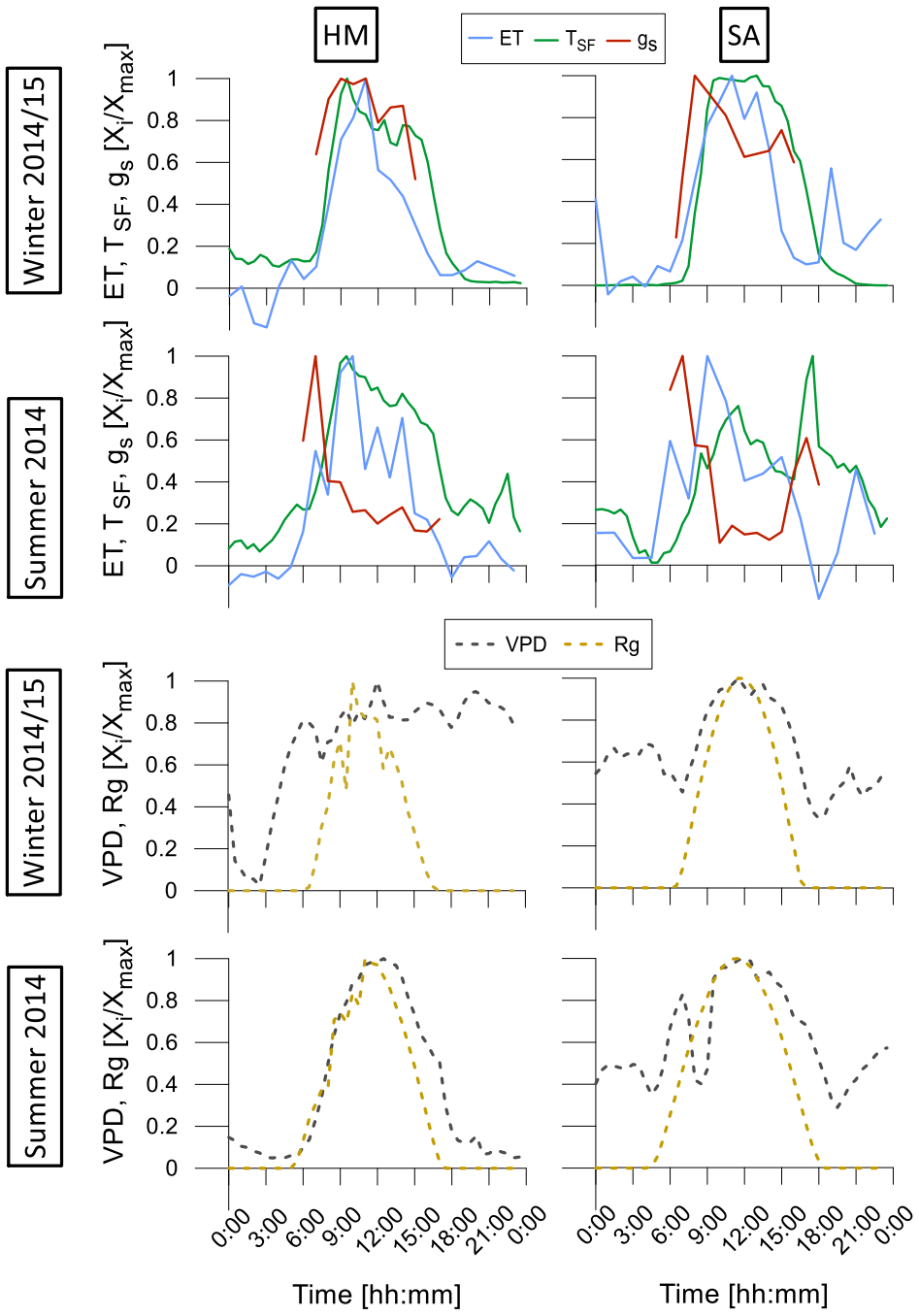

Fig 3.10. Daily patterns in water fluxes in Humid-Mediterranean (HM) and Semi-Arid (SA) forests: Results for HM (left plots) and SA (right plots) forests indicate ecosystem Evapotranspiration (ET, continuous light blue line), tree Transpiration up scaled from sap flow measurements (T_{SF}, continuous green line), and leaf stomatal conductance (g_s, continuous red line). Environmental conditions include vapor pressure deficit (VPD, dashed grey line), and global solar radiation (Rg, dashed yellow line). All fluxes and parameters are normalized for their daily maximum values. Diurnal curves are based on hourly data measured by three different methods: Eddy co-variance (ecosystem scale), sap flow sensors (tree scale), and leaf chamber gas exchange system (leaf scale). Data are from representative measurement day in winter (Jan 2015) and summer day (Jul or Sept. 2014, for the SA and HM forests, respectively).

4.4.2 Forest water fluxes from ecosystem to leaf scale

The next level of testing the interactions between ET and environmental conditions, was done by the comparisons of 3 scales water fluxes, from ecosystem (ET) to tree Transpiration (T_{SF}) and leaf scale (stomatal conductance to water, g_s), between the HM and SA forests ecosystems. Figure 3.10 presents the results from four intensive measurement days in Sept. and July in summer 2014 in HM and SA forest sites, respectively, and during the following winter (Jan. 2015). All parameters were normalized to their corresponding daily max, therefore, ranging between 0-1. During winter, ET daily patterns followed Rg during both days, essentially independent of changes in the VPD. During summer VPD seemed to play a more important role in influencing the daily patterns in ET. These daily patterns in ecosystem ET were quite distinct from the daily patterns in the tree and leaf scale fluxes (T_{SF} and g_s). Both T_{SF} and g_s values showed less pronounced daily curve and less positive relation with the daily patterns in the climatic parameters (Rg, VPD) in both seasons and ecosystems. In particular, g_s values showed distinct early morning peak in almost all cases, and a clear "mid-day depression" patterns in the SA site during summer time, probably reflecting physiological response to the very high VPD values at that time (approaching 3 kPa). As noted above, the results here clearly reflect the complex interactions of climatic and physiological factors on ET. In addition, the intensive campaigns with additional tree-scale measurements demonstrated the complex interactions between soil E and tree T on the total ecosystem ET, which is reflected in the decoupling between ET and tree T and g_s in the daily patterns reported in Fig. 3.10.

4.4.3 Additional trace gases within the forest ecosystem

The complex interactions between environmental conditions and forest water fluxes, reflected in the decoupling of ET diurnal trends noted above, could be demonstrate by additional trace gases such as O_3. Here we demonstrate the diurnal cycles of H_2O (ET), accompanied by total ozone flux (F_{O3tot}) above the canopy, partitioned to stomatal (F_{O3sto}) and non-stomatal (F_{O3ns}) fluxes (Fig 3.11). The HM and SA forests differ in both diurnal patterns and flux magnitudes across all three measured gases. However, while H_2O flux was higher in the HM site, O_3 fluxes were higher in the SA forest, when comparing to the HM (Fig 3.11). The diurnal pattern of F_{O3sto} showed sensitivity to high values of VPD, with early peak in the HM forest, and "mid-day depression" in the SA forest. This sensitivity to environmental conditions was less clear in the

ecosystem scale fluxes of ET and F_{O3tot}, demonstrating the decupling between physiological processes (such as stomatal ozone flux) and physical processes (including soil evaporation and ozone deposition), independently of the ozone concentrations.

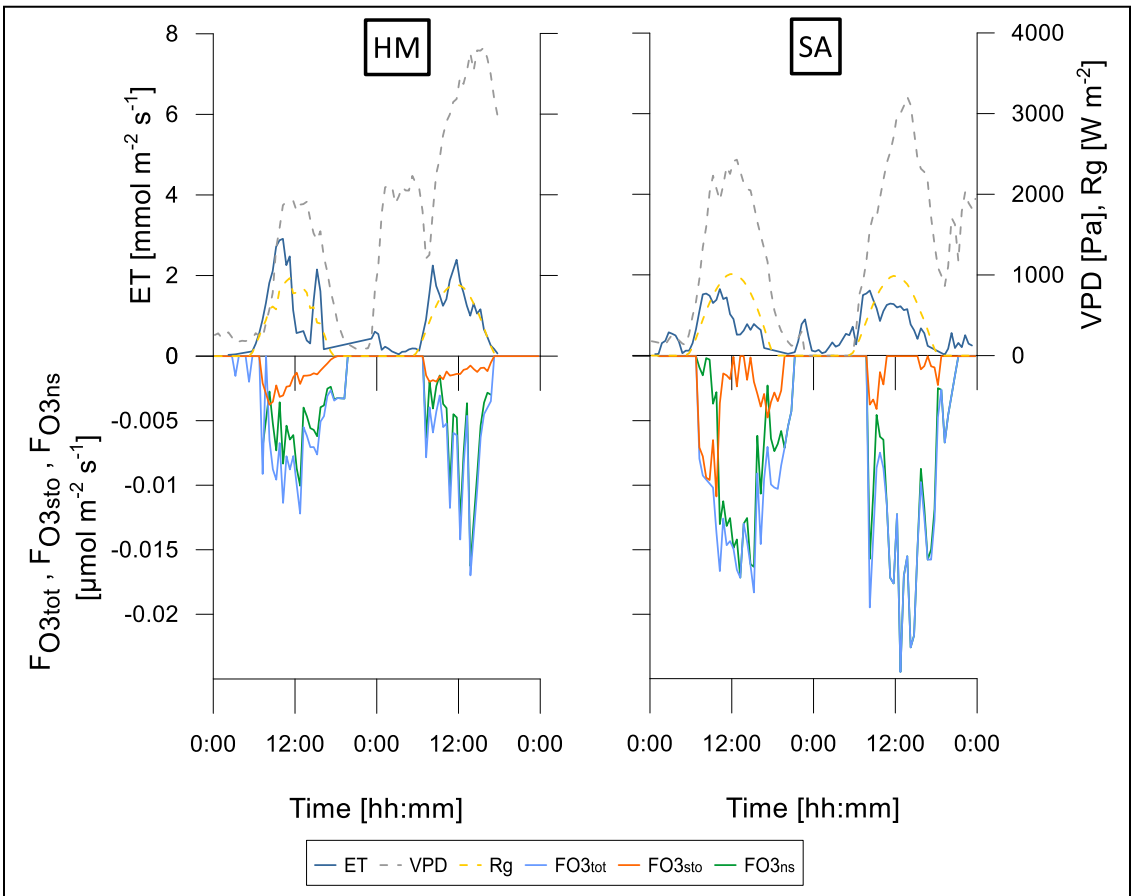

Fig 3.11. Daily patterns in gas exchange and O_3 fluxes in Humid-Mediterranean (HM) and Semi-Arid (SA) forests: Results for HM (Left plots) and SA (Right plots) forests indicate ecosystem gas exchange (Upper plots) of water flux by Evapotranspiration (ET, continuous blue line, and environmental conditions including, vapor pressure deficit (VPD, dashed grey line), and global solar radiation (Rg, dashed yellow line). The ozone flux partitioning include total ozone flux (F_{O3tot}, continuous light blue line), and its partitioning components of stomatal (F_{O3sto}, continuous orange line), and non-stomatal (F_{O3ns}, continuous green line) fluxes. Data are from representative measurement 2 days in summer (Aug or Sept. 2014, for the SA and HM forests, respectively).

4.4.4 Partitioning of forest water fluxes

Another attempt to demonstrate the complexity in water flux partitioning and the diurnal cycle of its components, was done using transpiration model, which is deriving transpiration (T_{gw}) through stomatal conductance to water on the canopy scale (g_w) and its functional relationship with gross primary production (for more details see 2.8 chapter at the method section). Diurnal changes at the SA forest, in ET, T_{gw}, and T derived from up scaled sap flow measurements (T_{SF}), shows significant differences in the diurnal patterns (Fig. 3.12a). While ET was following Rg, with

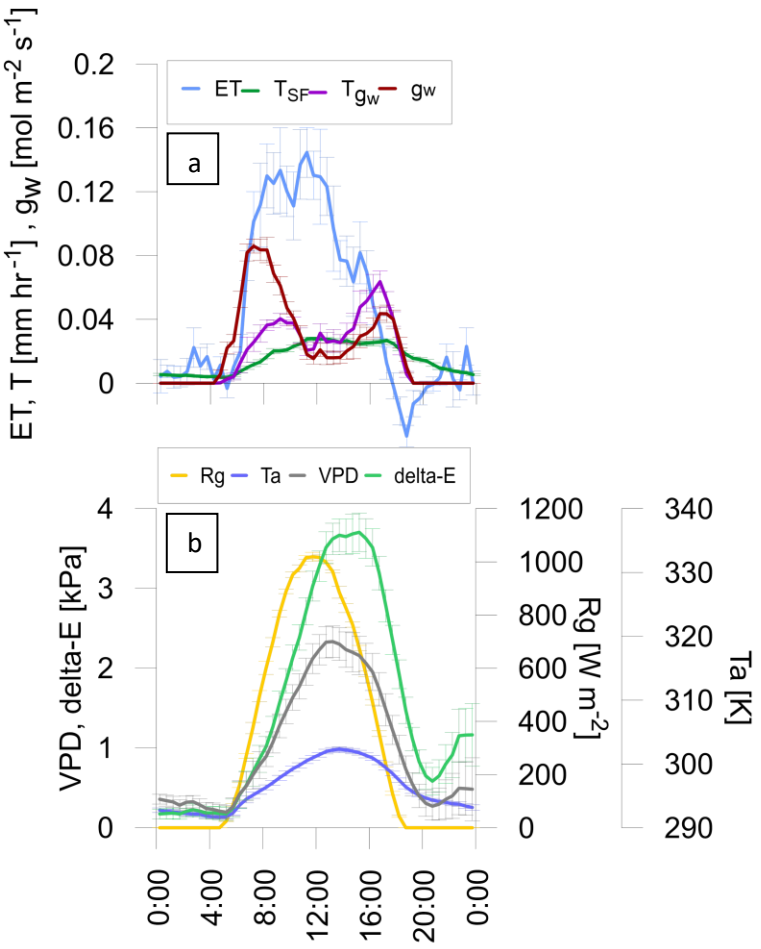

Fig 3.12 a- Averaged diurnal cycle of gas exchange at the Semi-Arid (SA) forest: Stomatal conductance at the canopy scale (g_w, red continuous line), Evapotranspiration (ET, light blue continuous line), Transpiration calculated from g_w (T_{gw}, purple continuous line), and Transpiration up-scaled from tree level sap-flow measurements (T_{SF}, green continuous line). **b- Averaged diurnal cycle of environmental conditions parameters:** Atmosphere Vapor Pressure Deficit (VPD, grey continuous line), Leaf scale VPD (delta-E, green continuous line), global Radiation (Rg yellow continuous line), and air Temperature (Ta, blue continuous line). Data measured and calculated from 15 days in July 2014 at the SA forest, error bars indicating the standard error of the means.

small shift of the peak to earlier morning, T_{SF} seems to follow delta-E (Fig. 3.12b), peaking around noon, and staying stable until late afternoon, finally decreasing into the evening hours, but with much more minor variations during the diurnal cycle, compared with all other physiological and meteorological parameters.

T_{gw} showed different pattern along the day, with small peak in the morning and higher peak in the afternoon, demonstrating the complex interaction between g_w, and the climatic parameters, in particular the leaf scale response to high values of atmosphere vapor pressure deficit (VPD). Although g_w and T_{gw} showed similar daily cycles of "mid-day depression" patterns, they differ in their peak timing. While conductance was higher in morning time, transpiration was higher in the afternoon hours, probably due to higher VPD in the afternoon (Fig. 3.12b). Environmental conditions represented here by air temperature (Ta) and calculated delta-E showed higher values in the afternoon when comparing to the early morning hours, different from Rg, which showed clear symmetric mid-day peak (Fig. 3.12b).

5 Discussion

This study investigates the changes in the water balance of forest and non-forest ecosystems under different land use and climatic conditions. For this investigation, we relied on a state-of-the-art mobile lab that proved to be of great importance in extending ecosystem flux data beyond the availability of one permanent flux-tower site, as was the case during the past 15 years. This permitted measurements and the investigation of additional land cover types and climatic conditions. The short-distance but steep climatic gradient and the mobile-lab platform enabled us to examine alterations in ecosystem water balance due to changes in land use, vegetation types and climatic conditions. Moreover, we demonstrated the ability to extrapolate seasonal results, ranging from the campaign-based measurements to annual continuous fluxes. This effort included direct measurements of ET by the mobile lab, the development and validation of methodology for the extrapolations of season-based measurements for the last 10-15 years, the partition of ET flux, and a comparative analysis of the hourly, daily and annual-scale results.

In general, the results indicate large differences in ET between land use types and between climatic regions, thereby demonstrating the need for a spatial extension of the permanent flux-tower methodological approach that is currently widely used. Moreover, the results indicate that an increase in ET is associated with afforestation, but this effect diminishes with a decreasing P. The results provide the first quantitative evaluation of the ET flux by the EC method, in the unique climatic gradient of Israel in association with afforestation, and have implications for forest management, ecosystem research, water balance, climate-change interactions with vegetation and climate-change modeling.

5.1 Israel's climatic gradient: Inter-annual variations

As noted above, this research focused on changes in ecosystem water balance that is associated with afforestation along the climatic gradient of Israel. The annual means from meteorological data that were collected for the three sites along the ICG confirm a clear gradient of the mean annual P, with a steep gradient of P and a mean annual P increasing from 284 mm yr^{-1} at the SA site to 479 mm yr^{-1} at the M site, and to 766 mm yr^{-1} at the HM site (Fig 1a). Other annual means of meteorological parameters did not show a significant gradient, but the two ends of the gradient (the SA and HM sites) show significant differences in all of the measured parameters, with the SA site showing higher Rg, VPD and Ta than the HM site. This was not the case for the moderate Mediterranean (M) site, which did not always follow the gradient. This led us to conclude that the limitation of the M site did not represent the gradient slope well due to its lower elevation of 380 m, compared to 650m and 755m at the SA and HM sites respectively (Table 2.1). Observations from the low elevation M site show a consistently higher T than in both the SA and HM sites, but no significant difference in Rg compared to the HM site, or in VPD compared to the SA site. This introduced unexpected complexity in using the M site as a mid-point for the climatic gradient and highlights the influence of the local geography on local climatic characteristics.

The North-South precipitation gradient was similar for the four years of measurement and the 10-15 previous years of archival data, thereby indicating that no significant change occurred over this period. This stands in contrast to the reported warming trend over the past several decades for this region (IMS-Israeli Meteorological Services). As expected, however, the inter-annual variations in P are large and the anomalies in annual P are very localized. For example, a

humid year in the northern part of Israel can be a dry year in the south and vice versa. This was strongly expressed during the four years of measurement: while the first two years show a linear increase in P, with an average increase of ~300mm from the drier to the next more humid site, the last two years show P anomalies, resulting in decreased differences between the HM and M sites. One exceptional hydrological year was 2013-14, which was an average year at the SA and M site, with 250 and 540 mm yr^{-1} respectively, but an extreme dry year at the HM site, with only 450 mm yr^{1}: 37% lower than its multiyear mean of 766 mm yr^{-1} and lower than the corresponding year's annual P at the M site. Notably, the prediction for the studied region is a decrease in the mean annual P in the north, and an increase or no change in the south (e.g., Steinberger & Gazit-Yaari, 1996; Ben-Gai *et al.*, 1998), though such trends are difficult to discern in light of the large inter-annual variations and frequency of P anomaly years.

5.2 The FMA approach

While the mobile lab that was used in this study enables the spatial expansion of the permanent flux-tower research, its measurements are limited to short-period campaigns. This requires an extrapolation methodology, in order to achieve continuous flux data that are critical for the assessment of hydrological budgets and ecosystems' response to change. We introduced here the flux meteorological algorithm (FMA), which is based on correlations between the meteorological parameters from nearby IMS stations and the fluxes that were measured by the mobile-lab system, and which successfully validated our approach.

An important validation and reliability test of the FMA approach was to test whether the campaigns during the four years of measurement represented the seasonality of the site well. This was particularly challenging because, in spite of major efforts to include all four seasons, the possibility existed of missing some key periods (e.g., the representation of the peak activity season in the non-forested HM site). However, Fig 3.3 shows that ~70% of the measurement days were captured within the standard-deviation range of a multi-year annual cycle, thereby supporting the assumption that short-term seasonal campaigns can provide a basis by which to estimate the local annual cycle. Notably, 30% of the measurements that were made outside the long-term SD range were made mostly in winter time at the HM sites, with a higher Ta and Rg, consistent with the relatively dry anomalies noted above. The importance of capturing the seasonal cycle and the peak-activity period was evident in the low representation of the active

season at the HM non-forested site, resulting in markedly lower regression coefficients (see Appendix Table A1).

An improvement of FMA's flux seasonality was clearly achieved by introducing a 'water availability index', as represented by the Transpiration Deficit, D (Eq. 13). This index appears to be required because the long drought periods in the studied region lead to periods in which the water availability imposes overriding control over ecosystem fluxes, thereby reducing the sensitivity to other meteorological parameter (e.g., VPD, Rg, T). The Transpiration Deficit is a good representation of the potentially available water for ET, which changes along the seasonal cycle as a dependence of cumulated P and PET. Differences in D between the sites are based on the sites' climatic conditions. In a preliminary comparison at the SA forest (data not shown), D seasonality shows a high correlation to that of available soil-water content (SWC is a missing parameter in the meteorological stations of the IMS). The introduction of D to the FMA regressions led to higher regression coefficients (about 20%) in all sites, and dramatically improved the FMA-based predictions of ET.

The FMA method was further tested by simulation experiments that were performed at the SA forest site, where continuous flux data from the permanent flux tower were available and where detailed comparisons of the FMA flux results can be made (see Appendix, Fig. A2). From the total daily data, 5% were selected stochastically by bootstrap. A quadratic stepwise regression was performed for this sample, followed by the prediction of fluxes for the whole observation period, using the equations obtained above (for more details, see appendix). This test confirmed our ability to predict continuous fluxes by using the FMA, based on the statistical regression of only 5% of the data (Fig. A2). Adding SWC data to the regression led to higher regression coefficients (about 10%) of the bootstrap results.

The extension of the method for the ICG sites was also validated, based on the comparison between FMA and the observations of ET (Fig. 3.6), which demonstrate a high consistency between both methods on the seasonal scale. For example, both methods indicate a higher ET at the forested sites and an increasing mean ratio of forest to non-forest ET, ranging from 1 during the wet season to ~2 during the dry season.

In summary, the FMA approach that was developed in this study is critical in extending the campaign-based measurements to the annual scale and we could validate its performance in different ways. We also demonstrated the importance of two main constraints for achieving high-quality results using the FMA approach: firstly, the representation of climatic conditions determined by well-planned short-term campaigns and secondly, the importance of using the 'water availability index' D in the dry environment, as a substitute for soil-water content.

5.3 Seasonality of ET in response to vegetation types and climate

The results demonstrate the importance of considering the strong interactions between seasonal and climatic conditions, and land-cover type. For example, the large seasonal effect can be reflected in greater ET values for the dry SA site in spring, compared to the wet HM site in summer. The strong climatic gradient effects on ET are prominent in spring and summer but are essentially eliminated in winter. Similarly, Lo´pez-Moreno *et al.* (2014) reported a decrease in forest streamflow mainly in late spring and summer, due to warming and drying trends in a more humid Mediterranean mountain. The drought effect on ET in the transition from spring to summer appears to be proportionally stronger at the driest SA site compared to the wettest HM forest site, with a ~50% vs. ~20% decrease in ET, respectively (Fig 3.6). The largest drought effect was observed in the dry SA NF site, where summer ET decreased to about 30% of the spring values, probably due to both low soil-water content and the absence of plants during the summer. The effect of the climatic conditions on forest activities changed with the seasons, with no significant difference among sites in the winter, but with a ~60% decrease in ET between the wettest HM to the driest SA forest. The highest proportional effect on ET appears to be the vegetation types during the dry season, with an increase in ET of ~200% and ~150% between the NF to F ecosystems, and the SA and HM sites, respectively. This proportional effect on ET at the seasonal time-scale demonstrates a high sensitivity of ET to climatic changes along the ICG and between seasons, and an even higher sensitivity of ET to vegetation type, changing from forest to non-forest ecosystems.

The interactions between water availability, and climate and vegetation type were also clearly reflected in the dynamics in the annual cycle of ET. As water availability decreases from the HM to the SA site, peak ET shifts from June to March, adjusting to the time of peak radiation and temperature that maximize evaporation. With decreasing water availability, the physiological

limitation to ET via reduced stomatal conductance becomes more important and results in a shift in peak ET toward the milder parts of the season. These results are consistent with other reports, such as those for the climatic effects on the peak timing of the water-balance components, streamflow and ET on a lower montane forest under Mediterranean climate conditions (Bart *et al.*, 2016). Using an eco-hydrologic model, this study shows a shift to an earlier increase in streamflow due to climate warming scenarios. Similarly, the greater capabilities of forest trees to mine water at depth enhance the water-availability effects noted above, resulting also in later ET peak time in the F compared to the NF ecosystems. This was highly expressed at the wet site, where ET peak time shifted from late May at the F site to late March at the NF site. This effect was less pronounced at the SA site, where the drought effect is very strong during the transition from spring to summer. An unusual behavior was observed at the NF SA site, with a small early-winter peak in ET (Nov-Dec, Fig. 3.7) that is probably associated to the early germination of seasonal annuals. Another exceptional behavior was observed at the HM NF site, with a much earlier peak of ET compared to the F site while under the same climatic conditions (late March compared to late May). This pronounced difference between the NF and F sites is likely associated with the heavy grazing at the NF sites, resulting in the earlier loss of leaf area during the peak season.

5.4 Afforestation and WYe

The results provided an opportunity to quantify the annual ET and, in turn, Wye, as well as their response to climatic conditions and vegetation type across the steep ICG. The multi-year average of annual ET (FMA-based, Table 3.1) indicates a 2.2 and 1.8-fold increase in ET for the F and NF sites respectively, across the ICG. This is probably due to the trees' deeper root system, which enhances water availability (e.g., Huxman *et al*., 2005). These differential climate-vegetation effects on ET also indicate a decrease from -200 to -58 mm yr-1 in the impact of forestation on WYe, which is associated with afforestation at the HM and SA sites. Noteworthy is the complementary relationships between the vegetation rain-use efficiency (ET/P) and the local WYe values (P-ET). As water availability decreases in dry sites, vegetation and forests particularly show an increase of rain-use efficiency, approaching 100% and diminishing WYe to near zero at the SA site.

The strong interactions between land-use change and climatic conditions on WYe are generally consistent with earlier studies based on modeling or with different vegetation types, scale and climatic conditions. For example, Liu *et al.* (2013) show a stronger impact of climate change on WY compared to the land-cover impact, based on their modeling study. Creed *et al.* (2014) used long-term experimental catchments to investigate different forest types' (such as conifer and deciduous) WY sensitivity to climate change, showing that conifer forests have a lower sensitivity to climate change (i.e., smaller changes in WY in response to climate change). Zhang *et al.* (2001) indicate that the annual ET is generally greater for forested than for non-forested (grassland) catchments, with larger differences in wet areas and diminishing in areas with an annual P under 500 mm yr^{-1}.

The results indicate two potentially important implications for local land use and hydrological managements. Firstly, the increase in ET (or decrease in WYe) that is associated with afforestation in the wet site was equivalent to ~30% of local P (Table 2). This quantifies a significant hydrological impact in water-limited regions such as the eastern Mediterranean, which is also sensitive to predicted climate changes (Oki & Kanae, 2006; Bates *et al*., 2008; Giorgi & Lionello, 2008; Jung *et al*., 2010). The results also indicate that such a hydrological impact is particularly important in the precipitation range of the study sites, approaching near maximum in the 700-800 mm range (Fig. 5). At this range, the ET of pine forests, such as those examined here, though possibly also in others (Zhang *et al.*, 2001; Bart *et al.*, 2016), is probably limited by stand density and leaf-area index, as well as by physiological controls (e.g., Maseyk *et al.*, 2008; Royer *et al.*, 2012; Sánchez-Costa *et al.*, 2015). The impact in the SA climate is markedly smaller (less than 20%) and far less significant in absolute quantity (58 mm). Such differences may imply different management tradeoffs between contrasting ecosystem services, such as WYe vs. carbon sequestration, local environmental conditions, desertification and recreation.

This study focuses on plantation forests that are dominated by *P. halepensis* trees, and on the interactions between ET, WYe and climatic conditions, and their comparison to adjacent non-forested sites. There is clearly a need to extend the results beyond pine forests in order to obtain a more comprehensive view of the effects of forestation on WY. During this study, a first attempt was made to introduce the mobile-lab platform to more diverse ecosystems, by

including preliminary measurements at a native oak forest, located at Ha'solelim in the western Galilee hills. The Appendix (Fig. A3) includes a report of the preliminary comparison of the ET flux between the native oak forest and the pine forest under similar Mediterranean climatic conditions. The results indicate that, under similar climatic conditions, the high-density pine forest and the low-density oak forest have similar ET levels during all seasons. In normalizing the results to the tree density, they indicate a higher water use by the oak trees compared to the pine trees, as expected from previous leaf-scale results (e.g., Klein *et al.*, 2013). Such significant differences in water use and ecosystem characteristics clearly indicate that there is limit to assessing vegetation effects on local hydrology on the basis of pine trees alone. Further exploring different vegetation and ecosystem types is clearly recommended.

5.5 Decoupling between ET and environmental conditions

The ET process combines physical and physiological effects. Under favorable conditions (e.g., high moisture availability), these effects are generally coordinated. But when conditions are unfavorable (e.g., water limitation), there is a decoupling between the physical effects that could enhance ET and endanger the plant, and the physiological controls that protect the plants and ensure their survival. Such a decoupling is clearly evident in the present study of ET under dry Mediterranean and semi-arid climatic conditions (Maseyk, 2006; Maseyk *et al.*, 2008; Raz-Yaseef et al, 2012).

For example, while an increase in Rg and VPD in transitioning from winter to spring is reflected in the large increase in ET, their further increase into the summer (reflected mainly by an increase in VPD) results in a decreasing ET (Fig 3.9). This must reflect the decrease in soil-moisture availability and the physiological adjustment of leaf-stomatal conductance to the combined effects of soil and atmospheric water stress. Furthermore, in the summer, inverse relationships between VPD and ET are observed in comparing ecosystems and sites, most prominently in the dry SA and wettest HM forest sites (Fig. 3.9). Similarly, on the diurnal time-scale, the time shift of ET peak to the early morning hours reflects a decoupling between ET and the climatic parameters, and must reflect an increasing dominance of physiological control over transpiration, via changes in stomatal conductance to water, g_w. It is also expected that soil evaporation, which is shown to be a significant fraction of ET in winter and spring (Raz-Yaseef *et*

al., 2012), greatly diminishes in summer due to dry-soil surface, thereby further enhancing the apparent leaf-scale control over the observed ET flux.

The results also indicate a higher seasonal sensitivity of the diurnal patterns of fluxes at all scales, ecosystem (ET), canopy (T_{SF}) and leaf (g_s), to shifting conditions from the wet to the dry season. This was overserved in comparing seasonality effects to changes from wet to dry sites (Fig. 3.10), though it should be noted that there is also a difference in seasonal changes between the three scales. It appears that, while the ET diurnal pattern generally follows Rg at the HM site and VPD at the SA site, the leaf response (g_s) was associated with high VPD values at both sites during the dry season, resulting in the decoupling of its diurnal pattern from that of the climatic parameters and from ET. Moreover, in both sites, T_{SF} diurnal pattern, like ET, appears to follow Rg until midday, but remains high until the early evening hours. This behavior can be associated to refiling and storage processes which contribute to some of the decoupling effects mentioned above (e.g., the use of storage for early morning ET. Tamir *et al.*, 2016).

The present study was carried out in parallel to a separate one focusing on ecosystem ozone fluxes. Ozone is an important atmospheric pollutant that can also cause damage to plants and influence physiological response (e.g., Burkart *et al.*, 2013). It is well known that ozone is taken up by leaves, both through the stomata and by deposition onto the leaf surface (Runeckles *et al.*, 1992). The availability of ozone flux data that are measured concurrently to our ET measurements offered another opportunity to examine the decoupling of physiological and physical effects on plant-atmosphere fluxes.

The partitioning of ozone flux to stomatal and nonstomatal flux indicates complex interactions between stomatal and total flux, and the climatic parameters (Fig. 3.11). Regarding g_s, stomatal ozone fluxes showed higher sensitivity to climatic factors, such as reduced flux in response to increasing VPD, compared to the total flux. This stands in contrast to the expectation that the total ozone flux increases in warmer and dryer conditions, which favor its formation and its deposition via biogenic volatile-organic compounds' (BVOCs) emissions (e.g., Goldstein *et al.*, 2004). Moreover, at similar VPD levels, diurnal patterns of ozone fluxes at the SA site showed sensitivity to the dry conditions with a typical 'mid-day depression' in fluxes that can be associated with a decrease in stomatal conductance. The contrast of large ozone and lower ET

fluxes at the SA site demonstrated an additional complexity in forest-gas exchange. While higher atmospheric concentrations of ozone and BVOCs at the SA site during the measurement period imposed higher ozone deposition fluxes, a limited availability of soil water results in a reduced stomatal ozone flux and ET flux (data not shown).

The dynamics in the evaporation fluxes were previously reported at the Yatir SA forest, indicating the decoupling between physiological processes, ET and T, and climatic parameters (e.g., Rg) under water-limited conditions (Raz-Yaseef *et al.*, 2012; Maseyk, 2006; Klein *et al.*, 2016). Here we add the key component of the evaporation flux dynamic, stomatal conductance to water (g_w), and demonstrate the difficulties in precisely evaluating the T flux in dry conditions, especially in the day to night transitions (see Fig. 3.12). However, the estimation of T fluxes was done through two independent methods (T_{SF} and T_{gw}) and showed agreement on the daily scale with previous research at the Yatir SA forest. For example, the T/ET ratios (0.33 and 0.39 based on T_{SF} and T_{gw}, respectively) that were calculated from the daily integral of Fig 3.12, were within the range of the previously report (0.3-0.6) for that site (Raz-Yaseef *et al.*, 2012).

The results indicate different mechanisms in the forest-water fluxes, and demonstrate the complexity in attempting to evaluate one flux in relation to the other (Fig. 3.12). As both a physiological and physical process, ET shows a typical diurnal pattern with an increase between morning and noon and a decrease in the afternoon, which is effected mostly by its energy engine, Rg. The stomatal flux, T_{gw}, which is a physiologically dominated process, shows a typical "midday depression" behavior, resulting from the stomatal-conductance response to environmental conditions, mostly with high VPD values. Finally, the non-continuous nature of the soil-plant-atmosphere pathway is demonstrated by the T_{SF} diurnal pattern, which increases until late afternoon, indicating a refiling and storage mechanism that helps to overcome the gaps between high atmosphere demand and stomatal flux, and low soil-water availability. It should be noted that certain unusual behaviors were observed in the late-afternoon diurnal patterns. The first regards the negative values of ET in the late afternoon, possibly associated with the condensation processes under high-humidity conditions, as previously reported for this site (Raz-Yaseef *et al.*, 2012). The second regards T_{gw} surpassing the total evaporative flux, ET, thereby indicating uncertainties in the conductance model, which is based on GPP that may

have different patterns in that part of the daily cycle. These anomalies demonstrate the difficulties of partitioning ET and the need to further improve these methodologies.

Concluding remarks:

Understanding the complex response of ET and its partitioned fluxes under changing climatic conditions is essential for evaluating the effect of land use and climate change on ecosystems' water yield. Our results indicate a strong sensitivity of forests' water cycle to changes in both climate and land use, and demonstrate the importance of quantification and of extend this research to more diverse ecosystems and climatic conditions. We conclude that afforestation is always associated with a loss in Wye, due to increased ET, but the afforestation impact on WYe is non-linear, diminishes with decreased precipitation and approaches saturation at high precipitation levels. These results provide an incentive to maintain or increase forestry in dry, or drying conditions, in order to benefit from ecosystem services other than WYe (e.g., carbon sequestration, wood production, surface cooling and recreation) and to carefully consider land-use changes on WYe in wet conditions. Our experimental approach based on the mobile lab proved to be an effective alternative to complex manipulation experiments and allows for the quantification of the effects of land-use changes during environmental changes, such as those that are associated with global warming.

6 References

Alcamo, J., Flörke, M., & Märker, M. (2007). Future long-term changes in global water resources driven by socio-economic and climatic changes. *Hydrological Sciences Journal*, 52(2), 247-275.

Alexandrov, Y., Balaban, N., Bergman, N., Chocron, M., Laronne, J. B., Powell, M., ... & Wener-Frank, I. (2008). Differentiated suspended sediment transport in headwater basins of the Besor catchment, northern Negev. *Israel Journal of Earth Science*, 57(3-4), 177-188.

Asaf, D., Rotenberg, E., Tatarinov, F., Dicken, U., Montzka, S. A., & Yakir, D. (2013). Ecosystem photosynthesis inferred from measurements of carbonyl sulphide flux. *Nature Geoscience*, 6(3), 186-190.

Aubinet, M., Grelle, A., Ibrom, A., Rannik, Ü., Moncrieff, J., Foken, T., ... & Clement, R. (1999). Estimates of the annual net carbon and water exchange of forests: the EUROFLUX methodology. *Advances in Ecological Research*, 30, 113-175.

Bart, R. R., Tague, C. L., & Moritz, M. A. (2016). Effect of Tree-to-Shrub Type Conversion in Lower Montane Forests of the Sierra Nevada (USA) on Streamflow. *PloS one*, *11*(8), e0161805.

Bates, B., Kundzewicz, Z. W., Wu, S., & Palutikof, J. (2008). Climate change and Water: technical Paper VI. Intergovernmental Panel on Climate Change (IPCC).

Beer, C., Reichstein, M., Tomelleri, E., Ciais, P., Jung, M., Carvalhais, N., ... & Bondeau, A. (2010). Terrestrial gross carbon dioxide uptake: global distribution and covariation with climate. *Science*, 329(5993), 834-838.

Ben-Gai, T., Bitan, A., Manes, A., Alpert, P., & Rubin, S. (1998). Spatial and temporal changes in rainfall frequency distribution patterns in Israel. *Theoretical and Applied Climatology*, 61(3-4), 177-190.

Bonan, G. B. (2008). Forests and climate change: forcings, feedbacks, and the climate benefits of forests. *Science*, 320(5882), 1444-1449.

Bren, L., Lane, P., & McGuire, D. (2006). An empirical, comparative model of changes in annual water yield associated with pine plantations in southern Australia. *Australian Forestry*, 69(4), 275-284.

Bronstert, A., Niehoff, D., & Bürger, G. (2002). Effects of climate and land-use change on storm runoff generation: present knowledge and modelling capabilities. *Hydrological Processes*, 16(2), 509-529.

Burkart S, Bender J, Tarkotta B, Faust S, Castagna A, Ranieri A, & Weigel HJ. (2013). Effects of ozone on leaf senescence, photochemical efficiency and grain yield in two winter wheat cultivars. *Journal of Agronomy and Crop Science*, 199(4), 275-285.

Cerdà, A. (1998). Changes in overland flow and infiltration after a rangeland fire in a Mediterranean scrubland. *Hydrological Processes*, 12(7), 1031-1042.

Cermak, J., Kucera, J., & Nadezhdina, N. (2004). Sap flow measurements with some thermodynamic methods, flow integration within trees and scaling up from sample trees to entire forest stands. *Trees*, 18(5), 529-546.

Collatz, G. J., Ball, J. T., Grivet, C., & Berry, J. A. (1991). Physiological and environmental regulation of stomatal conductance, photosynthesis and transpiration: a model that includes a laminar boundary layer. *Agricultural and Forest Meteorology*, 54(2), 107-136.

Creed, I. F., Spargo, A. T., Jones, J. A., Buttle, J. M., Adams, M. B., Beall, F. D., ... & Green, M. B. (2014). Changing forest water yields in response to climate warming: results from long-term experimental watershed sites across North America. *Global Change Biology*, 20(10), 3191-3208.

Dale, V. H., Joyce, L. A., McNulty, S., Neilson, R. P., Ayres, M. P., Flannigan, M. D., ... & Simberloff, D. (2001). Climate change and forest disturbances: climate change can affect forests

by altering the frequency, intensity, duration, and timing of fire, drought, introduced species, insect and pathogen outbreaks, hurricanes, windstorms, ice storms, or landslides. *BioScience*, 51(9), 723-734.

DeFries, R., & Eshleman, K. N. (2004). Land-use change and hydrologic processes: A major focus for the future. *Hydrological Processes*, 18(11), 2183-2186.

Dzikiti, S., Steppe, K., Lemeur, R., & Milford, J. R. (2007). Whole-tree level water balance and its implications on stomatal oscillations in orange trees [Citrus sinensis (L.) Osbeck] under natural climatic conditions. *Journal of Experimental Botany*, 58(7), 1893-1901.

Ehleringer, J. R. (2000). *Temperature and energy budgets*. In Plant physiological ecology (pp. 117-135). Springer Netherlands.

Ellison, D., N Futter, M., & Bishop, K. (2012). On the forest cover–water yield debate: from demand-to supply-side thinking. *Global Change Biology*, 18(3), 806-820.

Ewers, B. E., Mackay, D. S., Tang, J., Bolstad, P. V., & Samanta, S. (2008). Intercomparison of sugar maple (Acer saccharum Marsh.) stand transpiration responses to environmental conditions from the Western Great Lakes Region of the United States. *Agricultural and Forest Meteorology*, 148(2), 231-246.

Farley, K. A., Jobbágy, E. G., & Jackson, R. B. (2005). Effects of afforestation on water yield: a global synthesis with implications for policy. *Global Change Biology*, 11(10), 1565-1576.

Foken, T., Göckede, M., Mauder, M., Mahrt, L., Amiro, B. D., and Munger, J. W. (2004). Post-field data quality control, in: Handbook of Micrometeorology: A Guide for Surface Flux Measurement and Analysis, edited by: Lee, X., Massman, W. J., and Law, B., Kluwer, Dordrecht, 181–208.

Gash, J. H. C. (1979). An analytical model of rainfall interception by forests. *Quarterly Journal of the Royal Meteorological Society*, 105(443), 43-55.

Gerosa, G., Vitale, M., Finco, A., Manes, F., Denti, A. B., & Cieslik, S. (2005). Ozone uptake by an evergreen Mediterranean forest (Quercus ilex) in Italy. Part I: Micrometeorological flux measurements and flux partitioning. *Atmospheric Environment*, 39(18), 3255-3266.

Giorgi, F. (2006). Climate change hot-spots. *Geophysical Research Letters*, 33(8).

Giorgi, F., & Lionello, P. (2008). Climate change projections for the Mediterranean region. *Global and Planetary Change*, 63(2), 90-104.

Goldstein, A. H., McKay, M., Kurpius, M. R., Schade, G. W., Lee, A., Holzinger, R., & Rasmussen, R. A. (2004). Forest thinning experiment confirms ozone deposition to forest canopy is dominated by reaction with biogenic VOCs. *Geophysical Research Letters*, 31(22).

Granier, A., & Loustau, D. (1994). Measuring and modelling the transpiration of a maritime pine canopy from sap-flow data. *Agricultural and Forest Meteorology*, 71(1), 61-81.

Campbell, J. L., Driscoll, C. T., Eagar, C., Likens, G. E., Siccama, T. G., Johnson, C. E., ... & Buso, D. C. (2007). Long-term trends from ecosystem research at the Hubbard Brook Experimental Forest.

Huntington, T. G. (2006). Evidence for intensification of the global water cycle: review and synthesis. *Journal of Hydrology*, 319(1), 83-95.

Huxman, T. E., Wilcox, B. P., Breshears, D. D., Scott, R. L., Snyder, K. A., Small, E. E., ... & Jackson, R. B. (2005). Ecohydrological implications of woody plan encroachment. *Ecology*, 86(2), 308-319.

IPCC (2007). Contribution of Working Group 1 to the Fourth Assessment Report of the Intergovernmental Panel on Climate Change. In: IPCC, 2007. Climate change 2007. Eds. Solomon S, *et al.*, Cambridge University Press.

Israel Statistical Yearbook of 2014 (2015). The Central Bureau of Statistics (Israel). Israeli Government, http://www.cbs.gov.il/reader/shnaton/templ_shnaton.html?num_tab=st19_07&CYear=2014

Jung, M., Reichstein, M., Ciais, P., Seneviratne, S. I., Sheffield, J., Goulden, M. L., ... & Dolman, A. J. (2010). Recent decline in the global land evapotranspiration trend due to limited moisture supply. *Nature*, *467*(7318), 951-954.

Jones, H. G. (1998). Stomatal control of photosynthesis and transpiration. *Journal of Experimental Botany*, 49(Special Issue), 387-398.

Kaneti, T. (2010). Yield and physiological and environmental stress indices in persimmon trees irrigated with various grades of treated water. Thesis, the Hebrew University of Jerusalem, Rehovot, Israel.

Klein, T., Cohen, S., Paudel, I., Preisler, Y., Rotenberg, E., & Yakir, D. (2016). Diurnal dynamics of water transport, storage and hydraulic conductivity in pine trees under seasonal drought. *iForest-Biogeosciences and Forestry*, 9(5), 710.

Klein, T., Rotenberg, E., Tatarinov, F., & Yakir, D. (2015). Association between sap flow-derived and eddy covariance-derived measurements of forest canopy CO_2 uptake. *New Phytologist*, *209*(1), 436-446.

Klein, T., Shpringer, I., Fikler, B., Elbaz, G., Cohen, S., & Yakir, D. (2013). Relationships between stomatal regulation, water-use, and water-use efficiency of two coexisting key Mediterranean tree species. *Forest Ecology and Management*, 302, 34-42.

Kundzewicz, Z. W., & Takeuchi, K. (1999). Flood protection and management: quo vadimus? *Hydrological Sciences Journal*, 44(3), 417-432.

Lamaud, E., Loubet, B., Irvine, M., Stella, P., Personne, E., & Cellier, P. (2009). Partitioning of ozone deposition over a developed maize crop between stomatal and non-stomatal uptakes, using eddy-covariance flux measurements and modelling. *Agricultural and Forest Meteorology*, *149*(9), 1385-1396

Lelieveld, J., Hadjinicolaou, P., Kostopoulou, E., Chenoweth, J., El Maayar, M., Giannakopoulos, C., ... & Xoplaki, E. (2012). Climate change and impacts in the Eastern Mediterranean and the Middle East. *Climatic Change*, 114(3-4), 667-687.

Lindner, M., Maroschek, M., Netherer, S., Kremer, A., Barbati, A., Garcia-Gonzalo, J., ... & Lexer, M. J. (2010). Climate change impacts, adaptive capacity, and vulnerability of European forest ecosystems. *Forest Ecology and Management*, 259(4), 698-709.

Liu, Y., Zhuang, Q., Chen, M., Pan, Z., Tchebakova, N., Sokolov, A., ... & He, Y. (2013). Response of evapotranspiration and water availability to changing climate and land cover on the Mongolian Plateau during the 21st century. *Global and Planetary Change*, 108, 85-99.

López-Moreno, J. I., Zabalza, J., Vicente-Serrano, S. M., Revuelto, J., Gilaberte, M., Azorin-Molina, C., ... & Tague, C. (2014). Impact of climate and land use change on water availability and reservoir management: Scenarios in the Upper Aragón River, Spanish Pyrenees. *Science of the Total Environment*, *493*, 1222-1231.

Maseyk KS. (2006). Ecophysiological and phenological aspects of *Pinus halepensis* in an arid-Mediterranean environment. PhD thesis, Weizmann Institute of Science, Rehovot, Israel.

Maseyk, K. S., Lin, T., Rotenberg, E., Grünzweig, J. M., Schwartz, A., & Yakir, D. (2008). Physiology–phenology interactions in a productive semi-arid pine forest. *New Phytologist*, 178(3), 603-616.

Mastrandrea, M. D., Field, C. B., Stocker, T. F., Edenhofer, O., Ebi, K. L., Frame, D. J., ... & Plattner, G. K. (2010). Guidance note for lead authors of the IPCC fifth assessment report on consistent treatment of uncertainties.

McDowell, N., Pockman, W. T., Allen, C. D., Breshears, D. D., Cobb, N., Kolb, T., ... & Yepez, E. A. (2008). Mechanisms of plant survival and mortality during drought: why do some plants survive while others succumb to drought? *New Phytologist*, 178(4), 719-739.

McVicar, T. R., Donohue, R. J., O'Grady, A. P., & Li, L. T. (2010). The effects of climatic changes on plant physiological and catchment ecohydrological processes in the high-rainfall catchments of the Murray-Darling Basin: A scoping study. Prepared for the Murray-Darling Basin Authority (MDBA) by the Commonwealth Scientific and Industrial Research Organization (CSIRO) Water for a Healthy Country National Research Flagship, MDBA, Canberra, ACT, Australia.

Montgomery, R. B. (1948). Vertical eddy flux of heat in the atmosphere. *Journal of Meteorology*, 5(6), 265-274.

Moriondo, M., Good, P., Durao, R., Bindi, M., Giannakopoulos, C., & Corte-Real, J. (2006). Potential impact of climate change on fire risk in the Mediterranean area. *Climate Research*, 31(1), 85-95.

Ne'eman, G., and Trabaud, L. (2000). *Ecology, biogeography and management of Pinus halepensis and P. brutia forest ecosystems in the Mediterranean Basin*, Backhuys Publishers Postbus 321, 2300 AH Leiden, The Netherlands.

Noy-Meir, I. (1973). Desert ecosystems: environment and producers. *Annual review of ecology and systematics*, 25-51.

Obukhov, A. M., & Yaglom, A. M. (1959). On the microstructure of atmospheric turbulence–A review of recent work in the USSR. *Quarterly Journal of the Royal Meteorological Society*, 85(364), 81-90.

Ohmura, A. & Wild, M. (2002). Is the hydrological cycle accelerating? *Science*, 298:1345-1346.

Oki, T., & Kanae, S. (2006). Global hydrological cycles and world water resources. *Science*, 313(5790), 1068-1072.

Pachauri, R. K., Allen, M. R., Barros, V. R., Broome, J., Cramer, W., Christ, R., ... & Dubash, N. K. (2014). Climate change 2014: synthesis Report. Contribution of working groups I, II and III to the fifth assessment report of the intergovernmental panel on climate change (p. 151). IPCC.

Priestley, C. H. B., & Taylor, R. J. (1972). On the assessment of surface heat flux and evaporation using large-scale parameters. *Monthly weather review*, *100*(2), 81-92.

Runeckles, V. C., Chevone, B. I., & Lefohn, A. (1992). Surface level ozone exposures and their effects on vegetation. Crop Responses to Ozone. Ed. AS Lefohn. Chelsea, Mich: Lewis Publishers, Inc, 189-270.

Raz-Yaseef, N., Rotenberg, E., Yakir, D. (2010). Effects of spatial variations in soil evaporation caused by tree shading on water flux partitioning in a semi-arid pine forest. *Agricultural and Forest Meteorology*, 150, 454-462.

Raz-Yaseef, N., Yakir, D., Schiller, G., & Cohen, S. (2012). Dynamics of evapotranspiration partitioning in a semi-arid forest as affected by temporal rainfall patterns. *Agricultural and Forest Meteorology*, 157, 77-85.

Reichstein, M. *et al.* (2005).On the separation of net ecosystem exchange into assimilation and ecosystem respiration: Review and improved algorithm. *Global Change Biology*. 11, 1424-1439.

Roderick, M. L., & Farquhar, G. D. (2002). The cause of decreased pan evaporation over the past 50 years. *Science*, *298*(5597), 1410-1411.

Rotenberg, E., & Yakir, D. (2010). Contribution of semi-arid forests to the climate system. *Science*, 327(5964), 451-454.

Rosenberg, N. J., Blad, B. L., & Verma, S. B. (1983). *Microclimate: the biological environment*. John Wiley & Sons.

Royer, P. D., Breshears, D. D., Zou, C. B., Villegas, J. C., Cobb, N. S., & Kurc, S. A. (2012). Density-dependent ecohydrological effects of pinon–juniper woody canopy cover on soil microclimate and potential soil evaporation. *Rangeland Ecology & Management*, *65*(1), 11-20.

Sánchez-Costa, E., Poyatos, R., & Sabaté, S. (2015). Contrasting growth and water use strategies in four co-occurring Mediterranean tree species revealed by concurrent measurements of sap flow and stem diameter variations. *Agricultural and Forest Meteorology*, *207*, 24-37.

Shachori, A. Y and Michaeli, A., 1965. *Water yields of forests, maquis and grass covers in semi-arid regions: a literature review*, In Methodology of Plant Eco-Physiology, edited by F.E Eckart, pp.647-477. UNESCO, Paris.

Stanhill G (1993) In: Regional Implications of Future Climate Change. Proceedings of an International Workshop, Weizmann Institute of Science, Israel: pg 200.

Steinberger, E. H., & Gazit-Yaari, N. (1996). Recent changes in the spatial distribution of annual precipitation in Israel. *Journal of Climate*, 9(12), 3328-3336.

Steiner, J. L., Howell, T. A., & Schneider, A. D. (1991). Lysimetric evaluation of daily potential evapotranspiration models for grain sorghum. *Agronomy Journal*, *83*(1), 240-247.

Steppe, K., De Pauw, D. J., Doody, T. M., & Teskey, R. O. (2010). A comparison of sap flux density using thermal dissipation, heat pulse velocity and heat field deformation methods. *Agricultural and Forest Meteorology*, 150(7), 1046-1056.

Swinbank, W. C. (1951). The measurement of vertical transfer of heat and water vapor by eddies in the lower atmosphere. *Journal of Meteorology*, 8(3), 135-145.

Trenberth, K. E., Dai, A., Rasmussen, R. M., & Parsons, D. B. (2003). The changing character of precipitation. *Bulletin of the American Meteorological Society*, 84(9), 1205-1217.

Von Caemmerer, S. V., & Farquhar, G. D. (1981). Some relationships between the biochemistry of photosynthesis and the gas exchange of leaves. *Planta*, 153(4), 376-387.

Vörösmarty, C. J., Green, P., Salisbury, J., & Lammers, R. B. (2000). Global water resources: vulnerability from climate change and population growth. *Science*, 289(5477), 284-288.

Zhang, L., Dawes, W. R., Walker, G. R. (2001). Response of mean annual evapotranspiration to vegetation changes at catchment scale. *Water Resources Research*, 37: 701-708.

7 Appendix

7.1 The FMA approach – regression details and initial data

The FMA approach included a multiple linear stepwise regression between measured ET and meteorological parameter, which was applied for each of the ICG site, in order to express ET by one individual equation for each of the selected sites. The coefficient of each of the meteorological parameter at each site are summarized in Table A1. Both regression coefficient from the multiple stepwise regression (R^2reg.) and regression coefficient from the post regression of predicted vs. observed ET (R^2post), were highest at the HM forested site, where the largest amount of measurements days were available for the regression (N=52). The lowest R^2's were at the HM non-forested site (N=20).

Table A1. Summary of Flux Meteorological Algorithm (FMA) coefficients: output of the linear multiple stepwise regression between ET and meteorological parameters; global radiation (Rg, air Temperature (Ta), Relative Humidity (RH), Vapor Pressure Deficit (VPD), and seasonality index of transpiration Deficit (D), at five sites along the Israel Climatic Gradient; Humid Mediterranean (HM) and Mediterranean (M) forests, and there adjacent non-forested sites. The regression coefficient from the multiple stepwise regression (R^2reg.), and the regression coefficient from observation vs. predicted ET (R^2post) are presented for all five sites. N is the number of measurement days used for the regression at each site.

	Forest		Non-Forest	
	HM	M Pine	HM	M
Intercept	0.2904	0.7827	1.4390	1.4407
Rg (MJ m^{-2} d^{-1})	0.0928			0.0482
Ta (C°)		0.0540		-0.1093
RH (%)	-0.0161	-0.0159	-0.0114	
VPD (Pa)				0.0007
D (mm)	0.0015	0.0024	0.0014	
R^2 reg.	0.82	0.65	0.48	0.64
R^2 post	0.81	0.48	0.54	0.57
N	52	39	20	34

A specific equation from each site, based on the coefficients from table 6.1., was then applied at the continuous data set of meteorological parameters available from the 10-15 previous years. The results of four hydrological years, in which the measurements were conducted, are presented in Figure A1, demonstrating the seasonality capture by the FMA approach, with high agreement between ET from the FMA and observed ET.

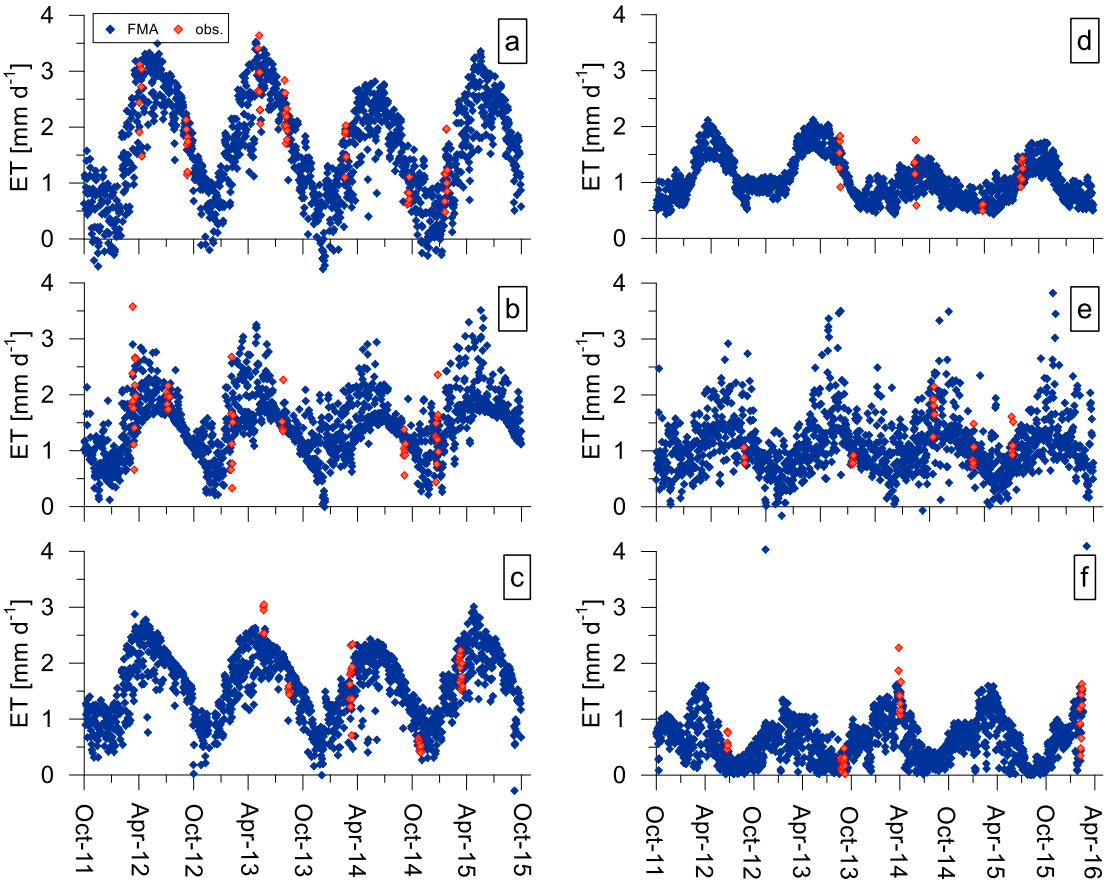

Figure A1. Observed and estimated ET: Continuous estimated daily ET from the Flux Meteorological Algorithm (FMA, blue closed diamonds) and observed ET (obs., red closed diamonds) by the eddy co-variance mobile lab, during four hydrological years of measurements, as calculated and measured in all sites along the ICG. Data are from 3 forests, Humid Mediterranean (HM) Pine forest (a), Mediterranean (M) Pine forest (b), and Mediterranean Oak forest (c), and from 3 non-forested sites, HM (d), M (e), and Semi-Arid (f).

7.2 Testing of Flux Meteorological Algorithm (FMA) using Yatir forest data.

Testing of the FMA was performed on the base of continuous Yatir data record using bootstrap method (selection stochastically subsamples from a finite population, in our cases all records of observations in Yatir. In this study, bootstrap sampling was used for deriving the regression of ET on meteorological variables. Daily totals (for fluxes and precipitation) or averages (for Ta, Rg, VPD, SWC) were used in this analysis. A fixed percent of days (5% or 10%) was selected stochastically from the whole dataset (only the records with no one of variables under consideration missing were used) and the stepwise multiple regression for each dependent variable was performed on the selected sample. Then the obtained set of regression coefficients was applied to the whole dataset to predict dependent variables and the R^2 between observed and predicted values was calculated (R^2_{post}). The procedure was repeated 20 times and finally regression R^2 and R^2_{post} for individual repetitions were averaged. The R^2 of prediction for mean values of regression coefficients was also calculated (if the coefficient was excluded by stepwise algorithm for a particular repetition, it was set to zero). Two multiple regression models were applied: linear and quadratic (including interaction terms $a_{ij}x_ix_j$). The Bootstrap results (Fig. A2)

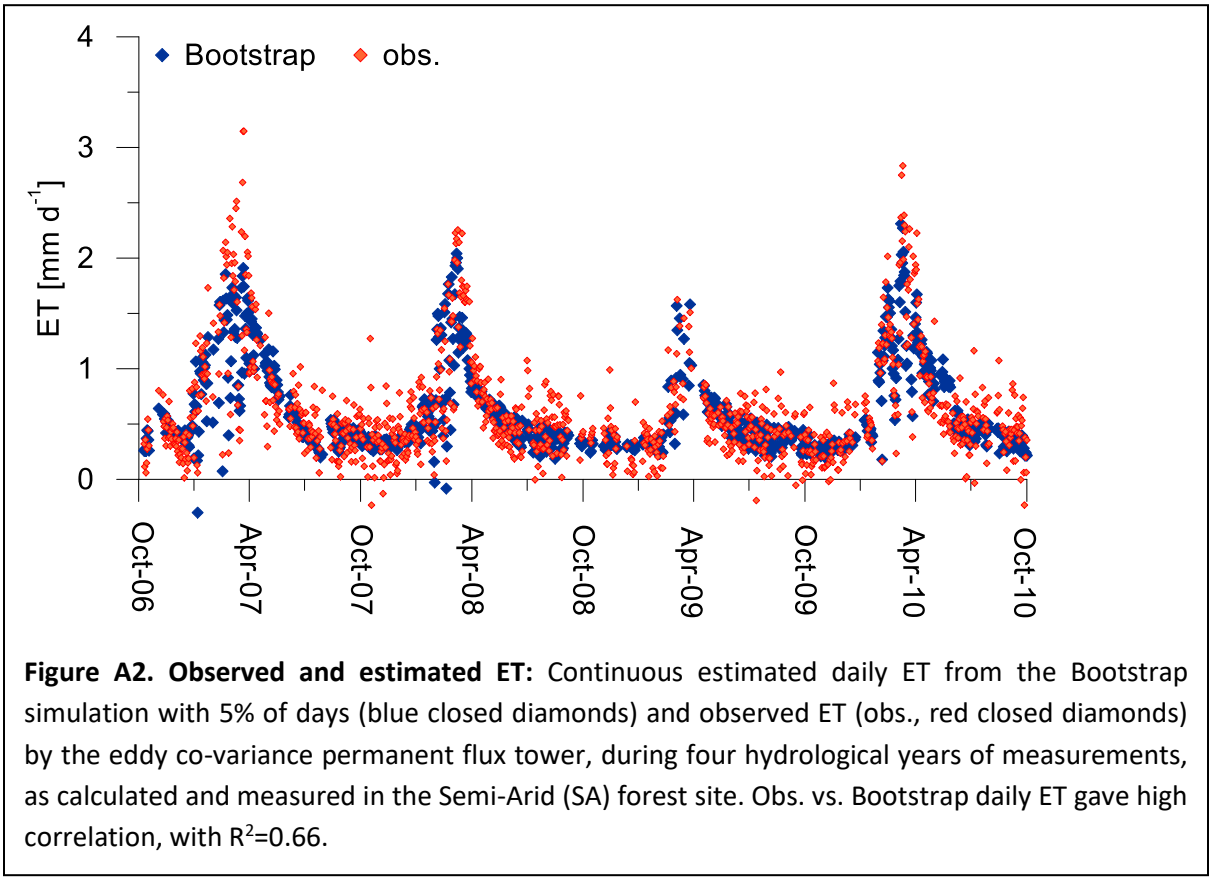

Figure A2. Observed and estimated ET: Continuous estimated daily ET from the Bootstrap simulation with 5% of days (blue closed diamonds) and observed ET (obs., red closed diamonds) by the eddy co-variance permanent flux tower, during four hydrological years of measurements, as calculated and measured in the Semi-Arid (SA) forest site. Obs. vs. Bootstrap daily ET gave high correlation, with R^2=0.66.

showed high correlation with the observed ET from the permanent flux tower, with high correspondence of seasonality, higher differences were observed on the daily scale ET, between predicted and observed.

7.3 Initial comparison between Pine and Oak forests

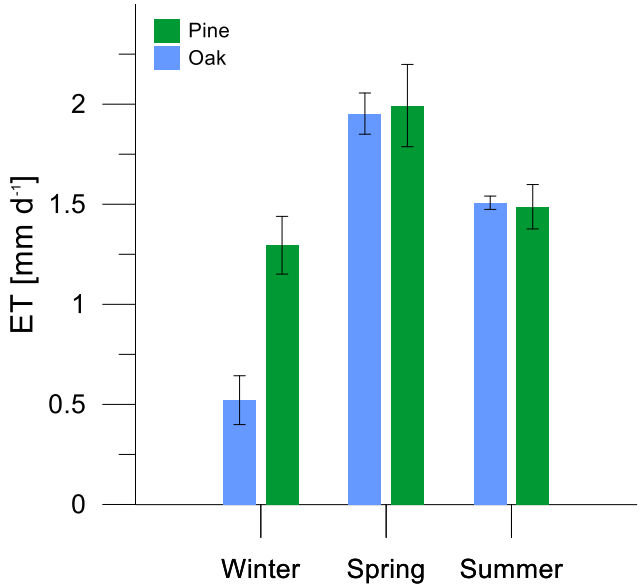

Figure A3. Observed daily ET from Pine and Oak Mediterranean forests in three seasons: Winter (Dec-Feb & Oct), spring (Mar-May), and summer (Jul-Sep). Observed daily ET fluxes were averaged by the 3 seasons periods from the campaign measurements, and were compared between Pine (green full bars) and Oak (purple full bars) Mediterranean forests. Standard error of the mean for measurement days is indicated.

The extension of this study from Pine forests to other forest types was conducted in a Mediterranean Oak (M_{Oak}) forest dominated by evergreen and deciduous). Measurements at the M_{Oak} forest were carried out throughout three years of research, and enabled us to make a preliminary comparison of the Pine vs. Oak type forests, on the ecosystem scale. The two forests showed similar levels of daily ET (Fig A3) during spring and summer time, but suffered much at winter. It is important to point out first, that winter data at the Oak forest were collected during the end of Oct. when the deciduous Oak species was already in a developed stage of fall, second, the two forest differ much in their density, with 480 trees ha^{-1} at the Pine forest and only 280 trees ha^{-1} at the Oak forest.

תקציר

בתהליך ההתאיידות (Evapotranspiration, ET) הצמחייה מאדה כמות מים משמעותית מכמות המשקעים השנתית (Precipitation, P) ולכן הנה בעלת השפעה גדולה על ההידרולוגיה המקומית. ההפרש הנותר [P-ET], מוגדר כמים הזמינים במערכת האקולוגית (ecosystem water yield, WYe), ומשמש כחלק ממקורות המים הטבעיים לצורכי האדם. מטרת המחקר הייתה לבחון את יחסי הגומלין בין השפעות שינוי כיסוי הצומח (ייעור) על כמות המים הזמינים, כתלות במשטר המשקעים (מאקלים לח/ים תיכוני לאקלים יבש/צחיח למחצה) ולזהות מנגנונים האופייניים ליחסי גומלין אלו. השערת המחקר הנה כי ייעור פני השטח, ובעקבותיו, הגדלת שטח העלים המאדה ועומק השורשים, מביא לעלייה בET וכתוצאה מכך לירידה בWYe. אולם, השפעה זו תצטמצם באופן יחסי עם הירידה בכמות המשקעים.

מדידות ההתאיידות במחקר זה, התבצעו מעל הנוף צמחי לאורך הגרדיאנט האקלימי של ישראל, ביערות אורנים נטועים בהשוואה לשטחים טבעיים סמוכים שאינם מיוערים וזאת בשלושה אתרים; בחבל יתיר בדרום (285 מ"מ ממוצע רב שנתי), באזור אשתאול (כ- 450 מ"מ) ובאיזור ביריה בצפון (755 מ"מ). מדידות שטפי מים (וכן פחמן, אנרגיה ואוזון) ומטאורולוגיה התבצעו על גבי תורן, המורם מעל התווך הצמחי בעזרת מעבדה ניידת. מדידות בשיטת קורלציית הערבולים (EC ; Eddy Covariance) מהוות את הבסיס למדידות השטפים. הרחבת השטפים מסדרות מדידה עונתיות, לשטפים רציפים ברמה השנתית וחישוב מאזני מים שנתיים, התבססה על הקשר בין השטפים למדדים מטאורולוגיים מתחנת מטאורולוגיות סמוכות, ופיתוח אלגוריתם המבטא קשר זה (Flux-Meteorologocal-Algorithm, FMA). מדידות פיזיולוגיות של קצב הטרנספירציה (T) ומוליכות הפיוניות (g_s) התבצעו על ידי מדידות זרימת המים בעצה (SF) ותאי מדידה לחילופי גזים בעלה, בהתאמה.

תוצאות המחקר מצביעות כי בתנאי היובש, כמות המים הזמינים הינה קטנה לעומת בתי הגידול הלחים. כמו כן, השפעת הייעור באקלים היבש הייתה מוגבלת והביאה לירידה בWYe מ 70 ל 12 מ"מ (58- מ"מ), בעוד שבתנאים הלחים, השפעת הייעור הייתה גדולה יותר, והביאה לירידה בWYe מ 344 ל 144 מ"מ (200- מ"מ). הבדל זה מקורו בעיקר בשל עלייה גדולה יותר בET במעבר מאקלים יבש ללח בשטחים המיוערים (מ 267 ל 583 מ"מ או פי 2.2) בהשוואה לשטחים הטבעיים הסמוכים ליער (מ 216 ל 383 מ"מ או פי 1.8). המחזור השנתי של ההתאיידות השתנה גם הוא לאורך הגרדיאנט, כאשר השיא ביערות נע מתחילת מרץ באקלים היבש לסוף מאי באקלים הלח. בשטחים הטבעיים הסמוכים ליער, שיא ההתאיידות נע מסוף פברואר לסוף מרץ, מאקלים יבש לאקלים לח, בהתאמה. סדרות המדידה העונתיות הצביעו על שינויים במהלך היומי של שטפי המים ברמות השונות (ET, T ו- g_s), כתוצאה משינויים בתנאי האקלים, המצביעים על שונות בהשפעת תנאי הסביבה (לדוגמה קרינה גלובלית, Rg, וגירעון לחץ האדים, VPD) ובהתאמות הפיזיולוגיות (לדוגמה SF ו- g_s).

מסקנות מחקר זה מראות כי בעוד ייעור מביא לירידה בWYe כתוצאה מעלייה בET, ההשפעה על WYe אינה לינארית ועולה עבור תנאים יבשים פחות, עד להגעה לרוויה תחת כמות משקעים גבוהה מספיק. תרומת עבודה זו יכולה להיות מסוכמת בנקודות הבאות: 1) המחשת יכולת השימוש במערכת מדידות חדשנית המתבססת על מעבדה ניידת וסדרות מדידה עונתיות; 2) פיתוח ואימות אלגוריתם על בסיס מדידות שטפים ומדידות מטאורולוגיות (FMA); 3) בהתבסס על 1 ו-2 הצגנו לראשונה הערכה מספרית של השפעת שינויי קרקע (ייעור) על המאזן ההידרולוגי המקומי תחת אקלים משתנה מלח ליבש, אשר אופייניים לתנאי הסביבה באזורינו. תוצאות אלו מספקות תמריץ נוסף להרחבה, או שימור היערות תחת תנאי אקלים בהן כמות המים הזמינים זניחה, וליהנות משירותי מערכת נוספים (לדוגמא, ויסות אקלים ע"י קיבוע פחמן, תעשיית העץ, בילוי בחיק הטבע).

שינויים במאזן האקו-הידרולוגי כתוצאה משינויים בשימושי הקרקע ובתנאי האקלים

עבודת גמר

מוגשת לפקולטה לחקלאות מזון וסביבה על שם רוברט ה. סמית

האוניברסיטה העברית בירושלים

לשם קבלת תואר

'מוסמך למדעי החקלאות'

על ידי

שני רוהטין

שבט התשע"ז **רחובות** **ינואר 2016**